Coordination Chemistry Reviews 424 (2020) 213520

Contents lists available at ScienceDirect

Coordination Chemistry Reviews

journal homepage: www.elsevier.com/locate/ccr

Metal-organic frameworks and their derivatives as signal amplification elements for electrochemical sensing

Shiyu Liu [a,b], Cui Lai [a,b,*], Xigui Liu [a,b], Bisheng Li [a,b], Chen Zhang [a,b,*], Lei Qin [a,b], Danlian Huang [a,b], Huan Yi [a,b], Mingming Zhang [a,b], Ling Li [a,b], Wenjun Wang [a,b], Xuerong Zhou [a,b], Liang Chen [c]

[a] College of Environmental Science and Engineering, Hunan University, Changsha 410082, PR China
[b] Key Laboratory of Environmental Biology and Pollution Control, Hunan University, Ministry of Education, Changsha 410082, PR China
[c] Faculty of Life Science and Technology, Central South University of Forestry and Technology, Changsha, Hunan 410004, China

ARTICLE INFO

Article history:
Received 4 March 2020
Accepted 24 July 2020

Keywords:
Metal-organic frameworks
Derivatives
Signal amplification
Electrochemistry
Sensing

ABSTRACT

Electrochemical sensor is a promising detection device with the characteristics of simplicity, rapidity, portability, and high sensitivity. With the increasing demands for ultrasensitive detection, extensive signal amplification strategies have been explored and developed to improve the performance of electrochemical sensor. Metal-organic frameworks (MOFs) hold enormous potential for electrochemical signal amplification owing to their attractive properties, including high porosity, superior surface area, unsaturated metal sites, and tunable structure and chemical functionality. In this review, we summarize the recent progress of MOFs and their derivatives as signal amplification elements in electrochemical sensing. Five different signal amplification routes of MOFs and their derivatives are systematically presented, including MOFs and their derivatives as support platforms, catalysts, carriers of signal elements, signal probes, and concentrators. Moreover, an outlook section of offering some insights on the future directions and prospects of MOFs and their derivatives in electrochemical sensing is highlighted with the purpose of conquering current restrictions by exploring more innovative approaches.

Contents

* Corresponding authors at: College of Environmental Science and Engineering, Hunan University, Changsha, Hunan 410082, China.
E-mail addresses: laicui@hnu.edu.cn (C. Lai), zhangchen@hnu.edu.cn (C. Zhang).

https://doi.org/10.1016/j.ccr.2020.213520
0010-8545/

1. Introduction

Electrochemical sensing is achieved by the change of electric signals stemmed from the reactions between the recognition elements on the electrode and target analytes [1]. Recognition elements and transduction elements, as key components of sensors, offer high identification for target analytes and transform the generated response into a measurable signal, respectively [2]. Electrochemical sensors can qualitatively and quantitatively analyze target analytes by integrating recognition elements and transduction elements. Due to its high sensitivity, simplicity, time efficiency, portability, and relatively low cost [3–6], electrochemical sensors are extensively employed in various fields, such as environmental monitoring [7], food safety control [2], clinical diagnosis [8], etc.

In recent decades, as the requirement for ultrasensitive detection has become urgent, researches on improving the response of electrochemical sensing through modification with various functional materials are increasing. So far, numerous micron materials and nanomaterials with diverse features have been applied to electrochemical sensing, containing metal nanoparticles (MNPs) [9,10], carbon nanomaterials [11–13], quantum dots [14,15], polymers [16], and semiconductor materials [17–19]. Thereinto, metal-organic frameworks (MOFs), as porous coordination polymers [20], possess many attractive merits of diverse structures, large specific surface area, high porosity, superior catalytic activity and adjustable physicochemical properties [1,7], which have aroused keen interest of researchers and realized a fast and remarkable progress in the field of electrochemical sensing. MOFs are composed of metal-containing nodes and organic linkers, and an extended infinite network is formed by self-assembly [21,22]. A wide variety of metal centers and organic ligands provide limitless possibilities for the structure and function of MOFs. The specific contributions of MOFs to electrochemical sensing are as follows: I) the high specific surface area of MOFs not only concentrates analytes to heighten the sensitivity of electrochemical detection [23], but also benefits the load of different functional materials (carbon nanomaterials, MNPs, biomolecules, etc.) or signal molecules (ferrocene (Fc), methylene blue (MB), etc.) for signal amplification; II) the catalytic active sites and redox activity brought by active metal ions or organic ligands endow MOFs with powerful electrochemical properties, which allow MOFs to be used as catalysts or even signal probes in electrochemical sensing [24]; III) the porosity of MOFs facilitates the introduction of guest materials [25] and provides size-selectivity for participating molecules [1]; IV) and host-guest interactions between MOFs and analytes, such as hydrogen bonding, van der Waals force, π-π interactions, covalent bonding, and electron donor/acceptor interactions, afford unparalleled selectivity for electrochemical detection [21,24].

Extensive reviews about MOFs and their applications in sensing have been summarized in recent years, including colorimetric sensing, luminescent sensing, and electrochemical sensing [1,7,20,26–30], etc. Especially, luminescent sensing applications of MOFs have been reported frequently. Nevertheless, systematic reviews of the use of MOFs in electrochemical sensing are rare. Several reviews on the applications of MOFs and/or MOF-based materials for electrochemical sensing have been published, and their topics primarily revolve around the structural design and composition design of MOF-based materials for electrochemical sensing applications [31], different MOF composites as electrocatalysts for electrochemical sensing applications [32], research progress of MOFs (as of 2017) in terms of sensing principles and analytical performance of electrochemical sensors [24], and application of MOFs as electrocatalytic electrode materials and signal

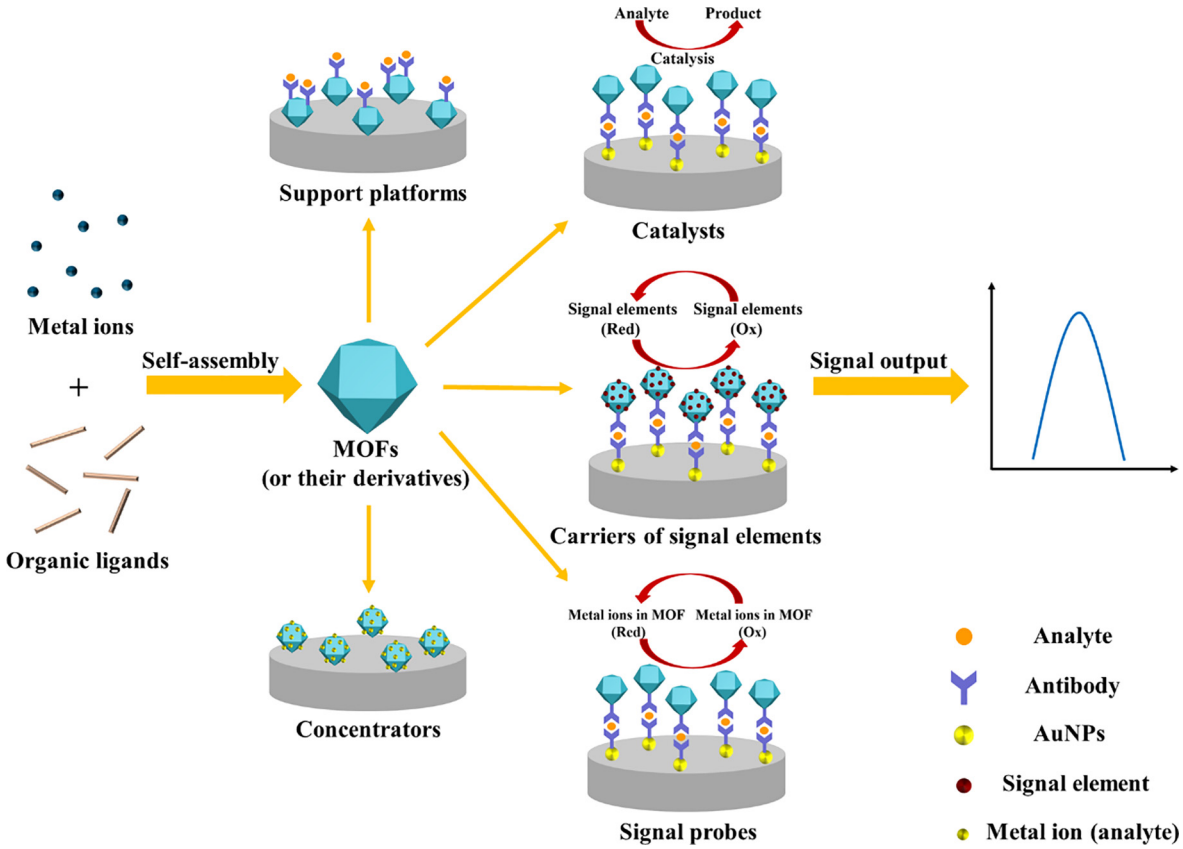

Scheme 1. Preparation of MOFs and schematic illustration of MOFs and their derivatives as different signal amplification routes in electrochemical sensing.

labels in electrochemical sensors and biosensors [33]. However, a comprehensive review of MOFs as signal amplification elements in electrochemical sensing is absent. In this review, we innovatively classify MOFs and their derivatives according to their different roles in electrochemical sensing from a unique perspective of signal amplification. Specifically, we focus on the recent progress of MOFs and their derivatives as signal amplification elements and classify the signal amplification routes according to their disparate role in electrochemical sensing. Five different routes of MOFs and their derivatives as signal amplification elements are systematically proposed and presented in Scheme 1. Briefly, MOFs and their derivatives can serve as support platforms, catalysts, carriers of signal elements, signal probes, and concentrators in electrochemical sensing. Thereinto, some representative and updated studies are adopted as typical cases and presented in this paper. Furthermore, the challenges and improvements of MOFs and their derivatives in electrochemical sensing are proposed with the goal of overcoming current limitations by exploring more innovative approaches.

2. MOFs and their derivatives as support platforms

In electrochemical sensors, numerous nanomaterials are utilized as electrode modifiers and carriers to load biomolecules for analytical performance improvement. The stable immobilization of biomolecules (such as aptamers and antibodies) at the interface of sensing device exerts a significant influence on electrochemical sensors. The number of immobilized biomolecules has a direct impact on the accuracy and sensitivity of sensors. Among the multitudinous nanomaterials, MOFs possess superior surface area, high porosity, and good biocompatibility, which make MOFs stand out as an ideal support platform for biomolecules fixation. These attractive properties of MOFs enable more biomolecules to be stably anchored on MOFs, further attaining amplificatory electrochemical signals.

Antigen-antibody reaction is the specific binding of antigen and corresponding antibody through non-covalent bonding, which possesses high specificity and is widely used for target recognition in the electrochemical sensing process. In view of the fascinating virtues of MOFs and antigen-antibody reaction, combining MOFs as sensing platforms and antigen-antibody reaction for target specific recognition is a feasible strategy for the construction of electrochemical sensors. On this basis, Du's group took advantage of two aluminum-based MOFs (Al-MOFs, 515- and 516-MOFs) as support platform for antibody adsorption, with the goal of food safety assessment [34]. The obtained two Al-MOFs had the advantages of large surface area, stable thermal and physicochemical properties, satisfactory electrochemical activity, and favorable biocompatibility. Nevertheless, the poor water stability of 515-MOF would lead to incompact bonding with electrode surface. Therefore, considering the reproducibility and stability of this immunosensor, 516-MOF was adopted as a sensing platform to load antibodies ($Anti_{vomitoxin}$ and $Anti_{salbutamol}$) for the determination of vomitoxin and salbutamol. The merits of 516-MOF and bio-recognition between antibody and antigen provided high selectivity and sensitivity for vomitoxin and salbutamol detection, with the limit of detection (LOD) of 0.70 and 0.40 pg/mL, respectively. In another study, Yu's team constructed a sandwich-type electrochemical immunosensor for monitoring galectin-3 (Gal-3, a biomarker of heart failure) by using a MOF-based nanohybrid as the substrate platform [35]. Owing to its strong stability and high surface area, Fe-based MOFs (Fe-MOFs) were selected and further modified by gold nanoparticles (Fe-MOFs@AuNPs) to obtain intensive conductivity and connect more primary antibodies (Ab_1) via Au-NH_2 interaction. Also, N-doped graphene nanoribbons (N-GNRs) were introduced via combination with Fe-MOFs@AuNPs for further enhancement of conductivity. The obtained nanohybrid (N-GNRs-Fe-MOFs@AuNPs) not only offered plentiful active sites for Ab_1 fixation, but also facilitated electron transport to enhance the sensitivity of the immunosensor. In addition, the rod-like AuPt-methylene blue nanocomposite (AuPt-MB), as a novel type of redox probe, was synthesized and applied to generate and amplify electrochemical signals for the first time. AuPt-MB was further decorated with the second antibodies against Gal-3 (Gal-3-Ab_2). In the presence of Gal-3, AuPt-MB approached the sensing interface through the sandwich type format formed by antigen-antibody identification, and an elevated signal response was attained with a low LOD of 33.33 fg/mL. Another sandwich-type electrochemical immunosensor was designed by Xu et al. for the analysis of lymphocyte activation gene-3 (LAG-3) protein based on an enzyme-free collaborative catalytic tactic and a signal-decreased label (Fig. 1) [36]. The matrix material of this immunosensor was constructed by the combination of AuPt alloys loaded Ni-Co hollow nanobox MOFs (HNMs/AuPt) and SnO_2-functinalized reduced graphene oxide (rGO-SnO_2). The formed rGO-SnO_2/HNMs/AuPt composite served as a support platform for loading antibodies and an electrocatalyst for catalytic reduction of H_2O_2 because of its increscent surface area, eminent conductivity, and brilliant electrocatalytic activity. Furthermore, the biotin-streptavidin system was employed to effectively immobilize antibodies due to the commendable specificity and affinity between biotin and streptavidin. Biotin-modified antibodies (Bio-Ab_1) were stably anchored on the surface of rGO-SnO_2/HNMs/AuPt via biotin-streptavidin reaction. Then, a signal-decreased label, SiO_2-tagged anti-LAG-3 antibodies (SiO_2-Ab_2) were introduced to promote the diminution of current signal and then increase the current difference, which was advantageous for enlarging the sensitivity of this immunosensor. In the presence of

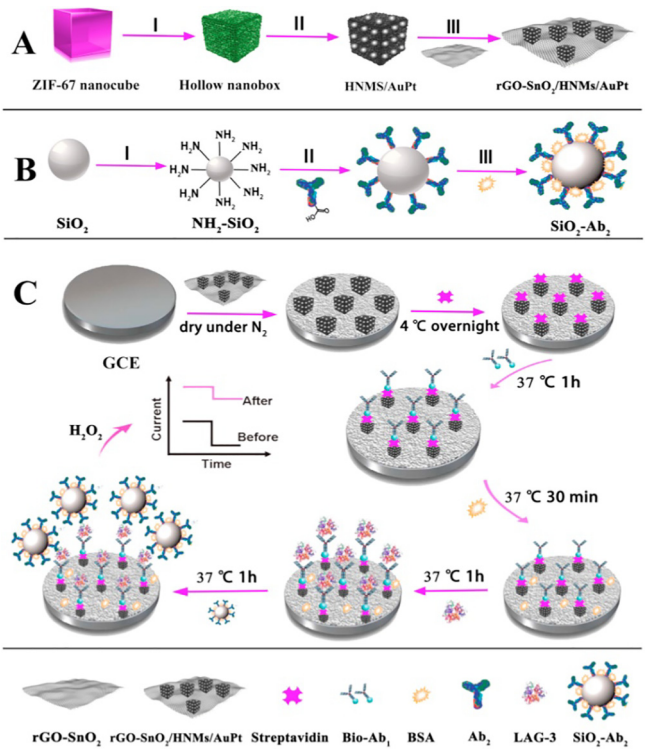

Fig. 1. Preparation of rGO-SnO_2/HNMs/AuPt (A) and SiO_2-Ab_2 (B), and schematic illustration of the electrochemical immunosensor fabrication process for LAG-3 protein detection (C). Adopted from Ref. [36]. Copyright 2018, with permission of Elsevier.

LAG-3, SiO_2-Ab_2 was attached to this immunosensor surface via antigen-antibody reaction, and a reduced current response was obtained due to large steric hindrance effect and suppressive electron transfer caused by SiO_2-Ab_2. By virtue of such an ingenious design, a satisfactory immunosensor was successfully built with the LOD as low as 1.1 pg/mL. In another example, a pyrolysis product of the Zn/Ni-bimetallic MOFs (Zn/Ni-ZIF-8-800) was exploited by Zhang's group as the scaffold material for monensin assay [37]. In order to acquire improved conductivity, a mixture of graphene and Zn/Ni-ZIF-8-800 (Zn/Ni-ZIF-8-800@graphene) was coated on the surface of the glassy carbon electrode (GCE), followed by electrochemical deposition of AuNPs to capture anti-monensin monoclonal antibodies. The formed mixture owned large surface area, remarkable electron transport capability, and praiseworthy biocompatibility by integrating the merits of Zn/Ni-ZIF-8-800 and graphene. With these virtues, a novel electrochemical signal amplification method was presented for monensin determination with the LOD down to 0.11 ng/mL.

Aptamers are single-stranded oligonucleotide sequences (DNA or RNA molecules), which exhibit high affinity and strong specificity to target analytes [5,38]. Compared with traditional antigen-antibody reaction, aptamer-based recognition systems demonstrate the merits of superior stability, easy to prepare and modify, and inexpensive cost [39], which make it more widely available for biological analysis. Hence, the integration of MOFs and aptamers for electrochemical sensing is another decent option. Inspired by this, Du's team designed a series of aptasensors based on the cooperation of MOFs and aptamers. Among them, a meaningful example was the electrochemical assay of lysozyme via three analogous Zr-based MOFs (Zr-MOFs) [40]. Zr-MOFs were chosen as the sensing platform owing to their eminent stability, low toxicity, and strong affinity for phosphate groups. Herein, three Zr-MOFs with adjustable pore characteristics were synthesized by regulating the terminal ligands. Three types of aptasensors were developed for lysozyme detection by employing three Zr-MOFs as support platforms. Aptamer strands were immobilized on the three Zr-MOFs surfaces through different binding patterns, including π-π stacking, hydrogen bond, and electrostatic force. Afterwards, the conformational change of aptamer chains was caused by the high binding affinity of aptamers with the target protein, which was monitored by electrochemical impedance spectroscopy (EIS) to quantify lysozyme concentration. Interestingly, Du et al. found that the binding modes of three Zr-MOFs with aptamers and lysozyme depended on the pore size and surroundings of Zr-MOFs. On this basis, the sensing performances could be well adjusted. Thereinto, a satisfying LOD of 3.6 pg/mL was achieved by the optimized Zr-MOF-based biosensor. In another example, two-dimensional (2D) Zr-MOF nanosheets embedded with Au nanoclusters (2D AuNCs@521-MOF) were synthesized by Du et al. as sensing platform for cocaine identification (Fig. 2a) [41]. The as-prepared 2D AuNCs@521-MOF combined the advantages of high affinity of Zr-MOF toward phosphate groups, large specific surface area of 2D nanosheets, and excellent electrochemical activity of AuNCs, which was utilized as a support platform for the attachment of cocaine aptamer chains. The conformational changes caused by the specific binding of cocaine aptamers to targets can further result in changes of electron transfer resistance, which can be monitored by EIS and differential pulse voltammetry (DPV) for cocaine quantification, with the LOD as low as 1.29 pM and 2.22 pM, respectively. Also, Du et al. prepared a battery of Zr-MOF composites by in-situ embedding three different aptamer chains in Zr-MOFs (509-MOF@Apt) for the direct analysis of thrombin (Tb), kanamycin and carcinoembryonic antigen (CEA), respectively [42]. As a result, three simple and well-performed aptasensors were fabricated via analyzing the conformational changes caused by the specific binding between aptamer chains

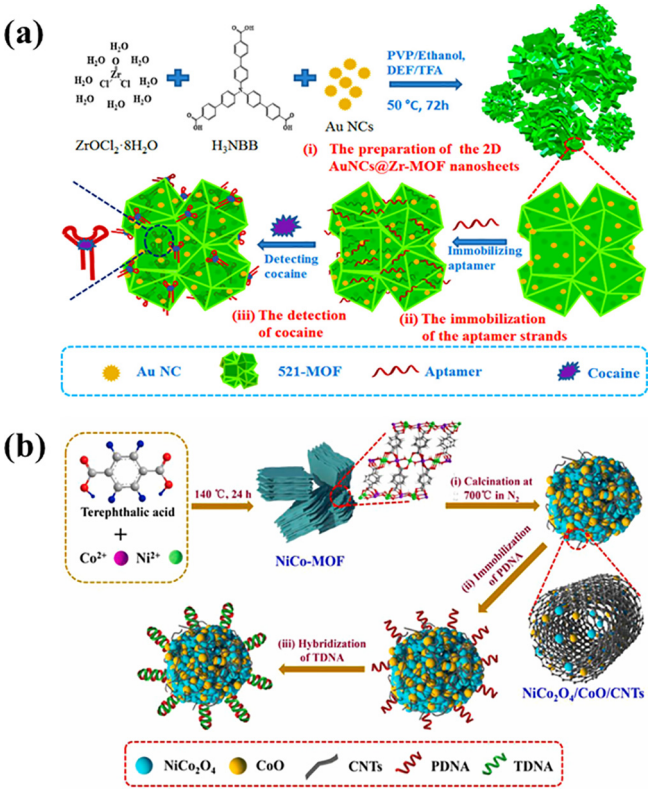

Fig. 2. (a) Schematic illustration of the fabrication process of electrochemical biosensing based on AuNCs@Zr-MOF-based nanosheets for cocaine detection. Adopted from Ref. [41]. Copyright 2017, with permission of American Chemical Society. (b) Schematic diagram of the fabrication procedure of the $NiCo_2O_4$/CoO/CNTs-based assay for detecting HIV-1 DNA. Adopted from Ref. [46]. Copyright 2019, with permission of Elsevier.

and target analytes, with the LODs of 0.37, 0.21, and 0.40 pg/mL for Tb, kanamycin, and CEA, respectively. In another study, Yu's team tactfully designed a sandwich-type biosensor for CYP2C19*2 gene assay by using AuNPs@Fe-MIL-88NH_2 (AuNPs@Fe-MOFs) as a sensing platform and a nanocomposite of CeO_2-functionalized carboxyl fullerene supported by Pt nanoparticles (c-C_{60}/CeO_2/PtNPs) as signal tag [43]. Biotin-modified capture probes (bio-CP) were anchored on AuNPs@Fe-MOFs through biotin-streptavidin reaction. Signal probe-labeled c-C_{60}/CeO_2/PtNPs were pulled closer to the electrode surface through a sandwich reaction of target gene with signal probe and capture probe. A distinct electrochemical response from the catalytic reduction of H_2O_2 by c-C_{60}/CeO_2/PtNPs was identified and further recorded by amperometry, and a gratifying LOD of 0.33 fM was attained. In view of the nanocomposite as signal tags and MOFs as sensing platforms, a similar sandwich-type aptasensor was presented by Bai's group for the detection of Mycobacterium tuberculosis MPT64 antigen [44]. A carbon nanocomposite (C_{60}NPs-N-CNTs/GO), with outstanding redox activity, excellent conductivity, and strong stability, was prepared by the integration of fullerene nanoparticles (C_{60}NPs), N-doped carbon nanotubes (N-CNTs), and graphene oxide (GO), subsequently decorated with AuNPs and then labeled with MPT64 antigen aptamer II (MAA II) to form a tracer label. Moreover, as support platform, polyethyleneimine (PEI)-doped Fe-based MOF (P-MOF) owned improved conductivity and was further modified with core-shell Au-Pt NPs (Au@Pt) for the dense attachment of thiolated MAA I. After the sandwich reaction and the addition of tetraoctylammonium bromide (TOAB), a significant electrochemical signal response was observed from the innate redox activity of the tracer label provoked by TOAB, and the calculated LOD was down to

0.33 fg/mL. Another fascinating study was proposed by Zhou et al. based on ZnZr bimetallic MOFs as a sensor scaffold for the analysis of protein tyrosine kinase-7 (PTK7, a cancer marker) [45]. An innovative MOF-on-MOF synthesis approach was explored for the preparation of ZnZr bimetallic MOFs. Two kinds of bimetallic ZnZr-MOFs, namely Zn-MOF-on-Zr-MOF and Zr-MOF-on-Zn-MOF, were successfully synthesized by changing the order of addition of metal precursors and ligands. In the constructed bimetallic ZnZr-MOFs, Zr-MOF was favorable for the fixation of aptamer chains, while Zn-MOF steadied the G-quadruplex derived from the specific recognition between the aptamer chains and PTK7. With such a clever combination, two aptasensors were developed for cancer marker sensing. Different MOF-on-MOF architectures led to diverse surface and electrochemical properties. Therein, the Zn-MOF-on-Zr-MOF displayed better sensing performances than Zr-MOF-on-Zn-MOF, with the LOD down to 0.84 and 0.66 pg/mL as determined by EIS and DPV, respectively. In a recent study, another bimetallic MOF, NiCo-based MOF (NiCo-MOF), was exploited by Jia et al. and further pyrolyzed to serve as a sensor scaffold for the assay of human immune deficiency virus-1 (HIV-1) DNA (Fig. 2b) [46]. It is worth mentioning that the impact of pyrolysis atmosphere on the composition and sensing properties of the prepared materials was studied. The results showed that different pyrolysis atmospheres (N_2 and H_2) would cause diverse nanostructures and chemical compositions of pyrolysis products, further affecting the fixation of probe DNA and the determination of target analyte. The pyrolysis product of NiCo-MOF under N_2 atmosphere ($NiCo_2O_4$/CoO@CNTs) was composed of $NiCo_2O_4$ spinel, CoO, metallic Co/NiNPs, and CNTs, while CNTs were absent in the pyrolysis product under H_2 atmosphere ($NiCo_2O_4$/CoO) due to the decomposition of organic ligands. Based on the synergistic effect between different components, $NiCo_2O_4$/CoO@CNTs nanocomposite displayed better sensing properties than $NiCo_2O_4$/CoO and was consequently chosen as the scaffold to immobilize the probe DNA for the determination of HIV-1 DNA. Profiting from the intrinsic virtues of $NiCo_2O_4$/CoO@CNTs, including remarkable electrochemical activity, favorable biocompatibility, and high affinity for the probe DNA, the proposed biosensor achieved an ultra-low detection with the LOD of 16.7 fM.

3. MOFs and their derivatives as catalysts

Natural enzymes are crucial biological macromolecules with highly efficient and selective catalytic activity. Nevertheless, the inferior stability, high production costs, complex preparation, and rigorous catalytic conditions of natural enzymes inevitably restrict their widespread applications [47]. As a decent substitute for natural enzymes, nanomaterials with enzyme-like properties (nanozymes) have drawn extensive concern owing to their easy production, low cost, and good stability [48,49]. Thereinto, MOFs are valued for their intriguing advantages, including multiple structures, adjustable pore sizes, and unique chemical composition, especially innate enzyme-mimicking catalytic activity, which make MOFs as good alternative to natural enzymes. In electrochemical sensing, MOFs as nanozymes can catalytically mediate signal amplification. The intrinsic catalytic activity of MOFs is derived from its own active metal sites or ligands. The periodic layout of metal nodes and organic ligands in MOFs supplies ample catalytic sites and gives MOFs innate enzyme-like catalytic activity [28]. Besides, the catalytic performance of MOFs can be effectively improved through some other modification ways, and the specific methods are listed as follows: 1) Functional modification of MOFs is a useful method to introduce the desired functions into MOFs by chemical means, which makes for the enhancement of catalytic activity of MOFs [1]; 2) The enhanced catalytic efficiency can be obtained by combining MOFs with catalytically active species, such as metal nanomaterials, enzymes, and electroactive molecules; 3) In general, most MOFs cannot meet the needs of electrochemical sensing due to low conductivity and chemical instability. Thus, constructing a composite of MOFs with highly conductive and mechanically stable materials is also an effective strategy to improve the electrochemical performance of MOFs [50]; 4) Furthermore, MOFs can be used as precursors or templates for the synthesis of MOFs derivatives. The obtained derivatives not only retain the inherent characteristics of MOFs to a large extent, but also acquire elevated stability and conductivity [51].

3.1. Pristine MOFs as catalysts

Metal ions embedded into the MOFs can catalyze the oxidation or reduction of different molecules and lead to the generation of electrochemical responses, which makes MOFs as promising catalysts in electrochemical sensing. Co, Cu, Zn, and Cr as common active metal nodes endow MOFs with powerful catalytic capacity. Zhang and co-workers prepared three types of 2D MOFs nanosheets by surfactant-assisted synthetic approach for H_2O_2 sensing [52]. Ultrathin bimetallic M-TCPP (Fe) nanosheets (sub-10 nm) were synthesized by using TCPP (Fe) as a heme-like ligand and M as metal nodes (TCPP (Fe) refers to Fe (III) tetra (4-carboxyphenyl) porphine chloride, M = Co, Cu, and Zn). Then, these 2D M-TCPP (Fe) nanosheets were employed as sensing platforms to determine H_2O_2. Thereinto, Co-TCPP (Fe) had optimal catalytic effect on the reduction of H_2O_2 with the LOD as low as 1.5×10^{-7} M. Furthermore, the proposed Co-TCPP (Fe) nanosheet-based sensor has been successfully applied to monitor H_2O_2 secreted by live cells in real time. In addition, Lopa et al. also proposed an enzyme-free method for electrochemical detection of H_2O_2 based on Cr-MOF (MIL-53-Cr^{III}), and the LOD was about 3.52 μM [53]. The obtained Cr-MOF was prepared by microwave assisted solvothermal approach and possessed prominent alkali stability. Cr^{3+} in Cr-MOF can be simply converted to Cr^{2+}, which directly mediated the catalytic reduction of H_2O_2. In another work, Ling et al. integrated conductive MOFs (Cu-MOF and Co-MOF) with flexible sensors for the detection of several important nutriments, including ascorbic acid (AA), L-tryptophan (L-Trp), glycine, and glucose [54]. Since the measured biomolecules can be oxidized by active metal sites in MOFs, the Cu-MOF modified sensor was capable of detecting AA, L-Trp, and glycine under different bias voltages with the LOD of 1.497×10^{-5} M, 4.14×10^{-6} M, and 7.1×10^{-7} M, respectively. While Co-MOF exhibited a better response to glucose due to its preferable catalytic activity. Thus, Co-MOF was employed for glucose sensing and a LOD of 5.46×10^{-5} M was obtained. The proposed implantable sensor can be applied to continuously track nutriments in organs, tissues and interstitial fluids with high sensitivity, selectivity, reversibility, and long life. Based on Cu-MOF (1,3,5-benzenetricarboxylic acid copper, $Cu_3(BTC)_2$), Dong's group constructed a simple and sensitive sensor for determining 2,4-dichlorophenol (2,4-DCP) [55]. Profiting from the good adsorption performance, enzyme-like catalytic property, and prominent electron conductivity of $Cu_3(BTC)_2$, a satisfactory LOD of 9 nM was attained.

3.2. MOFs with functional modification as catalysts

Chemical modifications of MOFs are elastic and available ways to introduce the required functions into MOFs. In a general way, MOFs are functionally modified by their metal nodes or/and organic linkers [1,28]. For instance, in the study of Lei's group, the Pt@UiO-66-NH_2 composite was constructed by one-step encapsulation of PtNPs into prototypal MOFs for tracing telomerase activity [56]. Thereinto, UiO-66-NH_2 was prepared by a

solvothermal method with 2-aminoterephthalic acid (NH_2-BDC) as the linker and Zr as the node. Fourier transform infrared spectroscopy (FT-IR) results manifested that UiO-66-NH_2 was successfully functionalized with amino groups. Benefiting from the combined merits of PtNPs and UiO-66-NH_2, the synthesized Pt@UiO-66-NH_2 composite displayed excellent electrocatalytic performance for $NaBH_4$ oxidation to get a detectable electrochemical signal. Based on the integrated design, a powerful platform for tracking telomerase activity was established with the LOD of 100 Hela cells mL^{-1}. In another example, a sequence of MOFs, including Fe-MOF, Co-MOF and NH_2-Co-MOF, were prepared by Wang et al., which exhibited inherent electrocatalytic activity for thionine (Thi) reduction without any substrate [57]. Interestingly, the results indicated that the electrocatalytic capability of three MOFs was structure-dependent and NH_2-Co-MOF possessed the highest electrocatalytic activity. The superb property of NH_2-Co-MOF should be ascribable to the following causes: (1) the circular trimeric metal unit of NH_2-Co-MOF effectually shaped a μ_3-O linked trigonal prism structure to promote electron transport; (2) the amino groups on its surface had a synergistic effect on catalytic capability of MOFs. Thus, NH_2-Co-MOF was selected as an example for the determination of Ochratoxin A (OTA). Furthermore, Exo I-assisted target recycling was introduced to further boost the detection sensitivity, and the LOD of the proposed biosensor was down to 0.3 fg/mL (Fig. 3a). Subsequently, Wang et al. further proposed a synthesis method of NH_2-Ni-MOFs with controllable size/morphology [58]. The size/morphology of NH_2-Ni-MOFs generally rested with the nucleation and growth process, which could be accurately controlled via altering the solvent and surfactant in the reaction system. An interesting experimental phenomenon was that the electrocatalytic activity for MB increased by nearly 2.7 times as the particle size decreased from 1.5 μm for NH_2-Ni-MOF(a) to 300 nm for NH_2-Ni-MOF(c). Hence, NH_2-Ni-MOF(c) was further applied to fabricate a sensing platform for C-reactive protein (CRP) analysis. Besides, an enzymatic cleavage powered DNA walker was introduced for amplifying the electrochemical signal (Fig. 3b). From the above, an amplificatory detection signal, with the LOD as low as 0.029 pg/mL, was earned based on the prominent catalysis of NH_2-Ni-MOF(c) and the aptamer binding induced DNA walker-antibody sandwich assay.

3.3. MOF-based composites as catalysts

3.3.1. MOF-metal nanoparticles composites as catalysts

MNPs, such as AuNPs, platinum nanoparticles (PtNPs), silver nanoparticles (AgNPs), palladium nanoparticles (PbNPs), and bimetallic nanoparticles, possess eminent enzyme-like catalytic ability [59,60]. Nevertheless, MNPs possess large surface energy, which results in their thermal instability and easy aggregation in the process of preparation and catalytic reactions [61–63]. The porosity of MOFs provides an advantageous platform for stabilizing MNPs. The pore structure of MOFs can be used for spatial constraint, preventing the aggregation and growth of MNPs [1,61]. Shen et al. proposed a ratiometric electrochemical sensor for detecting lipopolysaccharide (LPS) based on AuNPs functionalized Cu-MOFs (AuNPs/Cu-MOFs), and target-triggered quadratic cycles were also employed to amplify the electrochemical signal (Fig. 4a) [64]. In cycle 1, LPS triggered a conformational change of hairpin probes 1 (HP1) and the generated output DNA participated in the next cycle. In cycle 2, after the hybridization reaction of output DNA and ferrocene-labeled hairpin probes 2 (Fc-HP2), single-stranded capture probes were formed with the aid of N.BstNBI. Afterwards, capture probes were hybridized with AuNPs/Cu-MOFs labeled hairpin probes 3 (HP3). In the whole process, Cu-MOFs were introduced to the electrode surface through hybridization reaction, while Fc was far away from the electrode surface due to the cleavage of Fc-HP2, causing the signal enhancement of Cu-MOFs and the signal attenuation of Fc for ratiometric readout. Furthermore, in the presence of glucose, AuNPs/Cu-MOFs could catalyze the oxidation of glucose to achieve enzyme-free signal amplification, and a LOD of 0.33 fg/mL was realized. Here, AuNPs/Cu-MOFs simultaneously worked as a nanocarrier for the immobilization of HP3, an electroactive material for signal output, and a catalyst for glucose oxidation. Next, Shen et al. further constructed a dual-signal amplified electrochemical aptasensor for the determination of LPS based on AuNPs/Ce-MOFs and DNAzyme-assisted recycle [65]. As presented in Fig. 4b, LPS first reacted with the LPS aptamer of duplex DNA to form report DNA, then report DNA combined with hairpin probes 1 (HP1) to obtain Zn^{2+} dependent DNAzyme. With the aid of Zn^{2+}, the obtained DNAzyme cyclically incised HP1. After multiple cycles, the formed capture probe was hybridized with hairpin probes 2 (HP2) adsorbed on AuNPs/Ce-MOFs. AA, as an electrochemical substrate, was catalytically oxidized by AuNPs/Ce-MOFs for signal amplification, and a LOD of 3.3 fg/mL was obtained in this work. Furthermore, a Ce-MOF with mixed valence state, having an immanent catalytic ability for Thi reduction, was explored by Yu et al. to construct aptasensor for the determination of Tb [66]. Herein, proximity binding-induced DNA strand displacement and Exo III-assisted cyclic amplification were adopted for further sensitivity improvement. After DNA strand displacement triggered by Tb and Exo III-assisted cyclic amplification, a mass of single-stranded capture probes were generated. Then, Au-Thi-Au@Ce(III, IV)-MOF labeled hair probe 1 (HP1) was close to the electrode by hybridizing with the produced capture probes. The electrochemical reduction process of Thi was performed on Au-Thi-Au@Ce(III, IV)-MOF, and an enhanced current signal was acquired with the LOD as low as 0.06 fM. Notably, the high catalytic activity of Ce(III, IV)-MOF should be ascribable to the spontaneous circulation of Ce(III)/Ce(IV). Recently, Ren and his co-workers proposed a ratiometric electrochemical biosensor for probing telomerase activity based on Au@CeMOF tags and conformational change of hairpin DNA [67]. On the one hand, the conformation of MB modified hairpin DNA was switched, leading to a signal decrease of MB. On the other hand, Au@CeMOF tags were introduced to catalyze the oxidation of hydroquinone (HQ), and thus an increased HQ signal was generated. Ratiometric electrochemical sensing methods availably weakened the interference of background signal, and a LOD of 27 cells mL^{-1} was obtained.

In addition to AuNPs, some other MNPs have also been explored for MOFs modification. A core-shell heterostructure of PtNPs@UiO-66 was constructed by Xu's group for H_2O_2 quantification [68]. The core PtNPs encapsulated in UiO-66 (Zr-MOF) supplied plentiful active sites for H_2O_2 oxidation. And the shell UiO-66, with the triangular windows diameter of 6 Å, only allowed small molecules to transfer, which provided good size selectivity. At the same time, UiO-66 can effectively prevent PtNPs from aggregation. Thus, PtNPs@UiO-66 possessed prominent electrocatalytic activity to H_2O_2 reduction and superior anti-interference ability. As a result, a LOD of 3.06 μM was obtained. In another example, PdNPs were effectively adhered to the surface of iron-based MOFs via electrostatic self-assembly method, the formed nanohybrids (PdNPs@Fe-MOFs) were further applied by Li et al. to electrochemical sensing of microRNA-122 (miR-122) [69]. Herein, AuNPs-functionalized nitrogen-doped graphene sheets (AuNPs@N-G) were utilized as support platforms to load thiol-terminated capture probes (H_1). Besides, PdNPs@Fe-MOFs were employed as nanocarriers to immobilize biotin-labeled signal probes (H_2), and as tracers for the catalytic oxidation of 3,3′,5,5′-tetramethylbenzidine (TMB) in the presence of H_2O_2. Target miR-122, a biomarker of drug-induced liver injury, was sandwiched between H_1 and the tracers. On the basis of target-catalyzed hairpin assembly, miR-122 could initiate

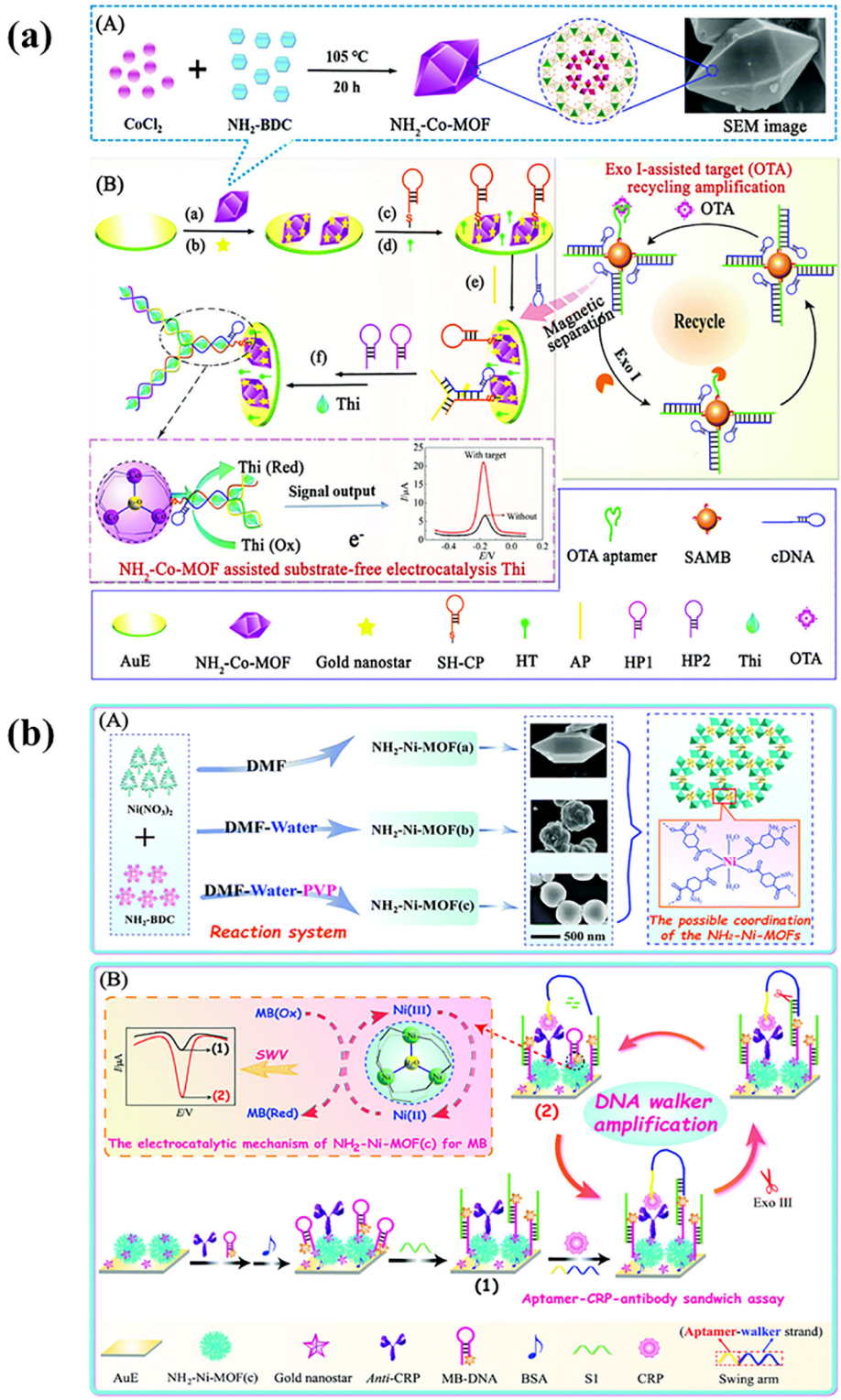

Fig. 3. (a) Schematic illustration of NH_2-Co-MOF preparation (A), and the electrochemical aptasensor fabrication process and NH_2-Co-MOF assisted substrate-free electrocatalysis for OTA detection (B). Adopted from Ref. [57]. Copyright 2017, with permission of Royal Society of Chemistry. (b) Preparation process of size/morphology-controllable synthesis of NH_2-Ni-MOFs (A), and the aptasensor fabrication process for CRP detection based on DNA walker and NH_2-Ni-MOF (c) assisted signal amplification (B). Adopted from Ref. [58]. Copyright 2018, with permission of Royal Society of Chemistry.

the hybridization of H_1 and H_2, then the released target participated in the next cycle. Thus, plentiful tracers were captured on the sensing interface, and an amplified signal response was attained with the LOD down to 0.003 fM. In another work, the ternary composites (MNPs@Y-1, 4-NDC-MOF/ERGO, M = Ag, Cu) were designed by Li et al. through first encapsulating MNPs into anionic MOFs (Y-1, 4-NDC-MOF) and then electrochemical reduction of graphene oxide (ERGO) [70]. The constructed ternary hybrids achieved satisfactory synergy for H_2O_2 detection by combining the catalysis of MNPs, the size selectivity of Y-1, 4-NDC-MOF,

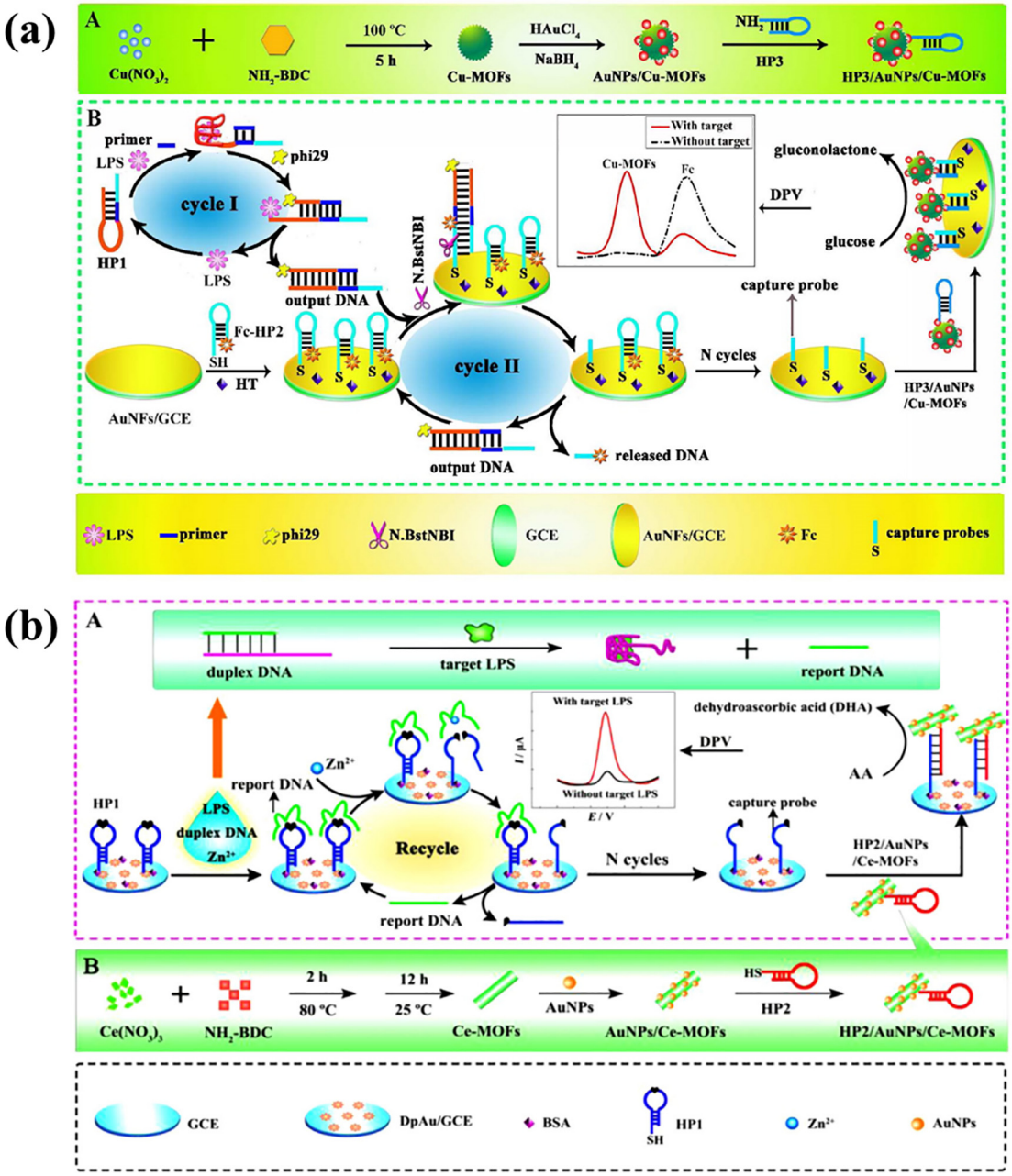

Fig. 4. (a) Preparation procedure of HP3/AuNPs/Cu-MOFs (A); and schematic diagram of ratiometric sensing of LPS based on AuNPs/Cu-MOFs and target-triggered quadratic cycles (B). Adopted from Ref. [64]. Copyright 2015, with permission of American Chemical Society. (b) Schematic diagram of electrochemical sensing of LPS based on AuNPs/Ce-MOFs and Zn^{2+} dependent DNAzyme-assisted recycling (A); and the preparation procedure of HP2/AuNPs/Ce-MOFs (B). Adopted from Ref. [65]. Copyright 2016, with permission of Elsevier.

and the conductivity of ERGO. Owing to faster electron transport rate, AgNPs@Y-1, 4-NDC-MOF/ERGO had better electrocatalytic performance for H_2O_2 reduction with the LOD of 0.18 μM. In a recent study, a novel synthetic method of Ag/MIL-160 hybrid was proposed by Dordick and his co-workers [71]. 2, 5-furandicarboxilic acid (FDCA) with photocatalytic properties was integrated into MIL-160 by coordination bonds connection of AlO_6 clusters, and then Ag/MIL-160 was obtained through photoreduction of Ag^+ under UV–vis light. Scanning electron microscopy (SEM) and transmission electron microscopy (TEM) analysis ascertained that a mass of AgNPs were successfully produced on the surfaces and inside of MOF. The resulting Ag/MIL-160 was highly sensitive to *p*-nitrophenol (*p*-NP) detection with a LOD of 0.04 μM. Noteworthily, the photocatalytic technology used in this study is recognized as a green and sustainable approach [72–74]. And the proper combination of photocatalytic technology and electrochemical sensing provides new ideas for the future development of these two fields.

Furthermore, bimetallic nanoparticles have been gradually developed to improve the performance of MOFs. A multi-enzyme system based on tandem catalysis of NiPd hollow nanoparticles and glucose oxidase (GO_x) was proposed by Zhang and his co-workers for glucose detection [75]. NiPd hollow nanoparticles and GO_x were concurrently fixed on the zeolitic imidazolate framework 8 (ZIF-8) by coprecipitation process, and thus GO_x@ZIF-8 (NiPd) nanoflower was formed. GO_x@ZIF-8(NiPd) nanoflower simultaneously possessed the peroxidase-like property of NiPd hollow nanoparticles and the intrinsic enzyme activity of GO_x,

which could be used not only for colorimetric sensing of glucose but also for electrochemical detection of glucose. Compared with colorimetric method (0.01–0.3 mM), a broader range of glucose detection was achieved by the electrochemical method (0.1–1.7 mM) based on competing reactions of oxygen reduction and glucose oxidation. He's team utilized PdPt alloys to modify Fe-MOFs (Fe-MOFs/PdPt NPs) for Pb^{2+} assay, and Pb^{2+}-specific DNAzyme was introduced to heighten the selectivity of sensing [76]. Besides, reduced graphene oxide-tetraethylene pentamine (rGO-TEPA) was employed as template for loading AuNPs and subsequently linked to streptavidin via covalent bonds, which acted as a sensing platform for DNAzyme immobilization. Fe-MOFs/PdPt NPs exhibited high catalytic activity for H_2O_2 reduction due to the synergistic effect of peroxidase-like performance of Fe-MOFs and catalytic capability of PdPt NPs. Hence, an amplified electrochemical signal was generated with a LOD as low as 2 pM. In addition, some reported MOF-metal nanoparticles composites as catalysts in electrochemical sensing are summarized in Table 1.

3.3.2. MOF-hemin composites as catalysts

Hemin, a famous natural metalloporphyrin, is the active center of hemeprotein family. Thanks to the reversible transformation of Fe(III)/Fe(II), hemin exhibits remarkable peroxidase-like catalytic activity [83]. Nevertheless, finite catalytic lifetime caused by the dimerization and oxidative self-destruction in aqueous medium restricts its application to a great extent [1,28]. An effective way to remedy these shortcomings is to anchor hemin on suitable carrier materials [84]. MOFs are ideal candidates for hemin fixation on account of regular structure and permanent porosity [85]. Integrating hemin into MOFs not only overcomes the dimerization and oxidative self-destruction of hemin, but also improves the catalytic performance and chemical stability of MOFs. For example, hemin was encapsulated into nano-sized Fe-MIL-88 MOFs (hemin@MOFs) and further applied for electrochemical sensing of Tb by Xie et al. [86]. Moreover, enzyme-assisted signal amplification method was introduced to enhance detection sensitivity (Fig. 5). The prepared multifunctional hemin@MOFs simultaneously served as a loading platform for the immobilization of biomolecules, a catalyst for H_2O_2 reduction, and a redox mediator for direct signal generation. With such an ingenious design, a low LOD of 0.068 pM was reached. He's team put forward a non-invasive electrochemical DNA sensor for determining FGFR3 mutation gene based on hemin encapsulated Fe-MIL-88 MOFs (hemin-MOFs) and biotin-streptavidin system [87]. FGFR3 mutation gene is a causative gene of achondroplasia, so early prenatal diagnosis of this gene is essential. In this study, AuNPs decorated rGO-TEPA was adopted as sensing platform with enhanced conductivity, and biotin-streptavidin system was introduced to immobilize capture probes (CP). Besides, PtNPs functionalized hemin-MOFs (hemin-MOFs/PtNPs) were utilized as signal amplification tags, which was capable of loading thiol-modified signal probes (SP) and achieving synergistic catalysis of PtNPs and hemin. After the addition of target DNA, hemin-MOFs/PtNPs was drawn close to the electrode surface due to the coupling of target DNA with CP and SP. Then, an obvious electrochemical signal from the catalytic reduction of H_2O_2 by hemin-MOFs/PtNPs was observed, and a low LOD of 0.033 fM was achieved. In another study, Song's group designed a nanocomposite through loading Cu-hemin MOFs on chitosan-reduced graphene oxide (CS-rGO) for H_2O_2 detection [84]. The Cu-hemin MOFs/CS-rGO nanocomposite possessed distinct peroxidase-like activity and improved electrical conductivity, which caused ideal electrochemical properties for H_2O_2 reduction and a LOD of 0.019 μM was obtained.

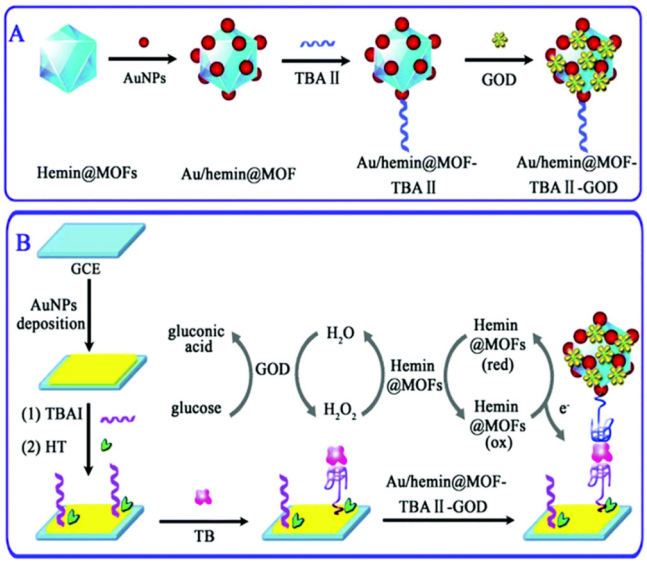

Fig. 5. The preparation of Au/hemin@MOFs conjugated with glucose oxidase and thrombin binding aptamer (Au/hemin@MOF-TBA II-GOD bioconjugates) (A); and schematic diagram of electrochemical sensing of Tb based on hemin@MOFs and enzyme-assisted signal amplification strategy (B). Adopted from Ref. [86]. Copyright 2015, with permission of Royal Society of Chemistry.

Table 1
Summary of the reported MOF-metal nanoparticles composites as catalysts in electrochemical sensing.

Catalyst	Sensing target	Linear range	LOD	Refs.
Au-SH-SiO_2@Cu-MOF	Hydrazine	0.04–500 μM	0.01 μM	[77]
AuNPs/Cu-MOFs	LPS	1.0 fg/mL-100 ng/mL	0.33 fg/mL	[64]
PtNPs@UiO-66	H_2O_2	5 μM-14.75 mM	3.06 μM	[68]
AuNPs/Ce-MOFs	LPS	10 fg/mL-100 ng/mL	3.3 fg/mL	[65]
AuNPs/MMPF-6(Fe)	Hydroxylamine	0.01–1.0 and 1.0–20.0 μM	0.004 μM	[78]
Fe-MOFs/PdPt NPs	Pb^{2+}	0.005–1000 nM	2 pM	[76]
AuNPs@Cu-MOFs	MicroRNA-155	1.0 fM-10 nM	0.35 fM	[79]
PdNPs@Fe-MOFs	MicroRNA-122	0.01 fM-10 pM	0.003 fM	[69]
Au-Thi-Au@Ce(III, IV)-MOF	Tb	0.1 fM-10 nM	0.06 fM	[66]
AgNPs@Y-1, 4-NDC-MOF	H_2O_2	4–11000 μM	0.18 μM	[70]
pSC_4-AuNPs/Cu-MOFs	Fractalkine	10 pg/mL-10 μg/mL	7.4 pg/mL	[80]
Cu-MOF/Au	Nitrite	0.1–4000 and 4000–10000 μM	82 nM	[81]
Ag@ZIF-67	H_2O_2	5.0–275, 775–2775 and 4775–16775 μM	1.5 μM	[82]
Au@CeMOF	Telomerase activity	200–2000000 cells/mL	27 cells/mL	[67]
Ag/MIL-160	*p*-NP	0.1–1.0 and 1.0–40 μM	0.04 μM	[71]

AuNPs/MMPF-6(Fe) refers to AuNPs-modified metal-metalloporphyrin framework, and pSC_4-AuNPs/Cu-MOFs represent para-sulfonatocalix[4]arene-coated AuNPs-functionalized Cu-MOFs.

3.3.3. MOF-carbon nanomaterials composites as catalysts

Although the seductive characteristics of MOFs suggest them as perfect electrode modification materials, a large percentage of MOFs cannot satisfy the needs of electrochemical sensing due to poor conductivity. Moreover, weak material characteristics cause the instability of most MOFs in aqueous media [88]. Fortunately, carbon nanomaterials, such as graphene, ordered mesoporous carbon (OMC), and CNTs, bring hope to the imperfections of MOFs owing to their complementary advantages with MOFs, including high conductivity and strong mechanical strength [89–91]. Integrating MOFs and carbon nanomaterials as composites is an effective strategy to improve the electrochemical performances of MOFs. The obtained MOF-carbon nanomaterials composites combine the merits of both MOFs and carbon nanomaterials, which compensates for the inherent insufficiency of MOFs.

Graphene, a 2D sp^2-hybridized carbon nanomaterial, can be used not only as a direct electrode material, but also as a good modifier for other electrode materials to improve the corresponding electrochemical properties, owing to its fantastic advantages of good conductivity, high surface area, and variable functional groups [92,93]. Wang et al. constructed a simulated multi-enzyme system by the combination MOFs with GO_x for glucose sensing, and graphene nanosheets were employed to obtain improved conductivity, preferable electrochemical activity, and larger accessible surface area [94]. Interestingly, a microcapsule was made of polydopamine (PDA) and ZIF-8 by using $CaCO_3$ as templates, which was applied to fix GO_x. Firstly, H_2O_2 was produced from the catalytic oxidation of glucose by GO_x. Then, the graphene nanosheets decorated PDA/ZIF-8 microcapsule, with significant electrocatalytic capability, catalyzed the reduction of H_2O_2 to H_2O. The generated electrochemical signal was recorded by amperometric measurements, and the LOD was estimated to be 0.333 μM. Similarly, Zhang et al. fabricated an electrochemical sensor based on chromium terephthalate MOFs (MIL-101(Cr) crystals) and rGO for monitoring 4-nonylphenol (4-NP) [92]. The introduction of rGO aimed to boost the conductivity of MIL-101(Cr) crystals. The enhanced oxidation current of 4-NP was acquired by using MIL-101(Cr)@rGO nanocomposite modified electrode, and the LOD was calculated to be 33 nM. Also, ZIF-67 (Co-MOF) was anchored on both sides of graphene nanosheets (GSs) by in-situ growth to form a sandwich-like composite, which was designed by Chen et al. and applied for glucose detection (Fig. 6a) [95]. GSs were prepared by physical exfoliating and further used to construct GS@ZIF-67 heterostructure. The resultant GS@ZIF-67 composite showed superior electrocatalytic property for glucose oxidation due to the synergistic effect of high catalytic activity of ZIF-67 and eminent electrical conductivity of GSs, and a LOD of 0.36 μM was earned. In a recent study, Cu-based MOFs (Cu-BTC) and ball-mill-exfoliated graphene were integrated in situ by Li et al. for monitoring different substances, including biomolecules and phenolic contaminants (Fig. 6b) [96]. The ball-mill-exfoliated graphene with high conductivity was applied for synergistic amplification of electrochemical activity of Cu-BTC. Benefiting from the improved activity, an electrochemical platform with high sensitivity was commendably constructed for multi-targets determination, and the satisfactory LODs of xanthine (XA, 0.0011 mg/L), hypoxanthine (HXA, 0.0073 mg/L), bisphenol A (BPA, 0.0012 mg/L), and *p*-chlorophenol (CP, 0.0019 mg/L) were achieved. In another research, Xie et al. prepared a composite of MOFs (ZIF-8) and graphene aerogels (GAs) by in-situ growth method for 2, 2-methylenebis (4-chlorophenol) (Dcp) measurement [97]. Furthermore, polypyrrole (PPy), a promising conductive polymer, was adopted as crosslinker to reinforce the bonding between ZIF-8 and GAs. Thanks to the combination of these three materials, the synthesized PPy@ZIF-8/GAs composite exhibited preeminent electrocatalytic activity for Dcp oxidation with the LOD down to 0.1 nM.

OMC is another powerful participant in electrode materials for its abundant mesopores, high surface area, desired conductivity, and good stability [98]. These characteristics also make OMC as an all-right option to promote the electrochemical performance of MOFs. Bo and his co-workers designed an electrochemical biosensor based on porphyrinic iron MOF (pFeMOF) and OMC for detecting H_2O_2 released from living cells [50]. pFeMOF was decorated on OMC by one-step hydrothermal method. The introduction of OMC not only reduced the aggregation of pFeMOF, but also strengthened the conductivity and stability of pFeMOF. Hence, an enhanced electrochemical activity for H_2O_2 reduction was obtained, and the LOD was calculated to be 0.45 μM. In the light of OMC-modified MOFs, Cu-MOFs were loaded on OMC by Wang et al. for hydrazine quantification [88]. The prepared Cu-MOFs/OMC hybrid showed remarkable electrocatalytic capability for hydrazine oxidation due to the integration of advantages of these two nanomaterials, and a LOD of 0.35 μM was achieved.

CNTs, with high surface area and eminent conductivity, were also normally utilized in electrochemical sensing. Bao's group employed an in-situ solvothermal route to construct Ni(II)-MOFs/CNTs composite and further applied it to H_2O_2 sensing [99]. The integration of conductive CNTs broke the limits of instability and weak conductivity of Ni(II)-MOFs. The synergistic catalytic activity of MOFs and CNTs was perfectly reflected on the sensing platform with the LOD down to 2.1 μM. In a recent research, Bai et al.

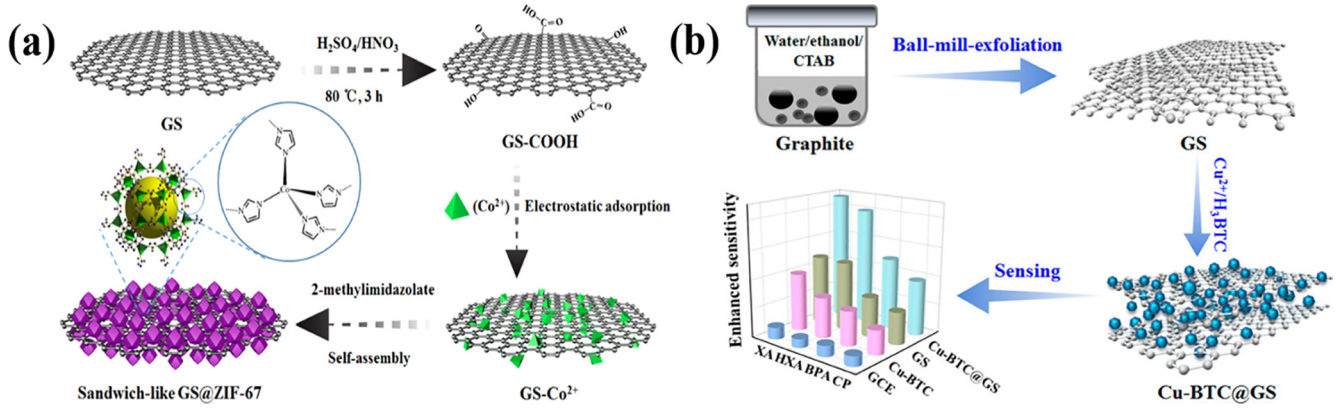

Fig. 6. (a) Illustration of the fabrication of sandwich-like GS@ZIF-67 hybrids and the application for glucose sensing. Adopted from Ref. [95]. Copyright 2019, with permission of American Chemical Society. (b) Integrating of Cu-BTC and ball-mill-exfoliated graphene as sensing platform for monitoring biomolecules and phenolic contaminants. Adopted from Ref. [96]. Copyright 2019, with permission of American Chemical Society.

prepared a series of ultrathin 2D MOF M-TCPP (M = Cu, Co, Ni) nanofilms and corresponding nanosheets by a simple surfactant-assisted bottom-up strategy for biomimetic enzymes and supercapacitor applications [100]. GO and CNTs were introduced to conquer the restrictions of pristine 2D MOF, including weak conductivity and easy agglomeration. Specifically, single-wall CNTs and GO were employed as growth matrix of 2D M-TCPP nanofilms (1D-2D M-TCPP nanofilms/CNT) and nanosheets (2D-2D M-TCPP nanosheets/GO), respectively. For biomimetic enzymes applications, 1D-2D M−TCPP nanofilms/CNT and 2D-2D M−TCPP nanosheets/GO acted as catalysts to construct H_2O_2 sensing platforms, and Cu-TCPP nanofilm/CNT possessed optimal catalytic ability for H_2O_2 reduction with a LOD as low as 5 nM. However, Ni-TCPP nanofilm/CNT showed first-rank performances in supercapacitor applications. Except for these carbon nanomaterials listed above, Meng et al. introduced acetylene black (AB) as conductive additive to boost the electrocatalytic property of Cu-MOF [101]. The as-prepared Cu-MOF/AB modified electrode achieved an improved electrocatalytic activity for H_2O_2 determination, and a low LOD of 0.014 μM was acquired.

3.3.4. Other MOF-based composites as catalysts

Similar to carbon nanomaterials, conducting polymers emerge as a promising candidate for overcoming the poor conductivity of MOFs on account of its outstanding conductivity, inexpensive cost, and effortless polymerization. Chen et al. designed a core-shell structure hybrid by coating poly(3-methythiophene) (P3MT) on the surface of metalloporphyrin MOF (PCN-222(Fe)) for levodopa (L-dopa) sensing [102]. The porous PCN-222(Fe) as core provided electrocatalytic sites and size/shape-selectivity, while P3MT polymer as shell facilitated charge transfer to the electrocatalytic sites. By combination of the superiority of PCN-222(Fe) and P3MT, a splendid sensing platform for L-dopa analysis was fabricated with the LOD down to 2 nM. Analogously, another core-shell structure composite was prepared by Wang and his co-workers for quercetin (QR) detection [103]. The difference is that the conductive polymer PPy served as the core while ZIF-8 acted as the shell. Benefiting from the remarkable electrocatalytic activity of ZIF-8 and the charge collection of PPy, the synthetic PPy@ZIF-8 composite exhibited amazing electrocatalytic activity for QR quantification with a LOD as low as 7 nM.

In addition, MOFs can be applied to the immobilization of biomacromolecules, such as enzymes, owing to their rich pores, large surface area, and good biocompatibility. MOFs can efficiently prevent the agglomeration and leakage of enzymes to improve their bioactivity and stability. For example, Lu and his co-workers employed Cu-MOF as matrix to immobilize tyrosinase for BPA sensing [104]. The prepared three-dimensional (3D) Cu-MOF, with a high surface area, facilitated the immobilization of enzyme and the preconcentration of BPA. For one thing, Cu-MOF supplied sufficient binding sites for tyrosinase fixation and the immobilized tyrosinase specifically catalyzed the oxidation of BPA. For another, the enhanced preconcentration of BPA was due to the π-π stacking interactions between BPA and Cu-MOF, which increased the available BPA concentration to react with tyrosinase. As a result, this biosensor showed superb performances for BPA detection, and an enhancive redox current derived from the enzyme-catalyzed reaction at the electrode interface was observed with a low LOD of 13 nM. Subsequently, Lu et al. further explored the electrochemical response characteristics of Cu-centered MOF (CuMOF) based tyrosinase biosensor to BPA and eight BPA structural analogues [105]. In this study, CuMOF and tyrosinase were immobilized on the GCE surface with the help of chitosan, and the electrochemical response characteristics of nine bisphenols (BPs) were systematically investigated. Interestingly, the proposed biosensor showed significant current response to bisphenol E, bisphenol F, BPA, bisphenol B, and bisphenol Z, while no response was found in tetrabromide BPA, bisphenol AP, bisphenol S and bisphenol AF sensing. An important conclusion drawn from the analysis of experiment results was that the electrochemical response of BPA and its structural analogues to the proposed biosensor was influenced by the molecular structure (especially the available ortho positions of phenolic hydroxyl groups) and the characteristics of substituent group (electron acceptor or donor) on the bisphenol framework. The substituent group had an impact on the electron cloud distribution of phenolic hydroxyl group, which decided whether the available ortho positions of phenolic hydroxyl group could be oxidized by tyrosinase. In another example, Zhang et al. constructed ZIF-8 with both mesoporous and microporous channels to load cytochrome *c* (Cyt *c*) for H_2O_2 quantification [106]. Compared to native Cyt *c*, the Cyt *c* loaded on ZIF-8 exhibited an improved apparent substrate affinity toward H_2O_2 and enhanced enzyme activity because the combination of mesoporous and microporous structures promoted substrate transport. Thus, an increased sensitivity for H_2O_2 detection was attained, which was 1.4-fold higher than that of native Cyt *c* modified electrode.

3.4. MOF derivatives as catalysts

To cover the shortages of weak conductivity and poor chemical stability of most virgin MOFs, it's a decent solution to convert MOFs into metal compounds, carbon-based materials or their composites by post-treatment methods [107]. Multiple functional materials can be prepared by using MOFs as self-sacrificial templates or precursors. These MOF-derived functional materials might inherit fine qualities of pristine MOFs to a certain degree, such as high surface area and rich pores. More importantly, MOF derivatives may give rise to diverse superiorities, containing elevated conductivity and stability. Zeng's group synthesized a Cu_xO nanoparticles@ZIF-8 (Cu_xO NPs@ZIF-8) composite derived from core-shell MOFs for H_2O_2 detection [108]. Depending on the disparate thermal stability of the two MOFs, an ideal core-shell heterostructure of Cu_xO NPs@ZIF-8 can be successfully constructed via direct pyrolysis of Cu-based MOF [nHKUST-1]@ZIF-8 (Fig. 7a). ZIF-8 was used as shell to protect Cu_xO NPs from agglomeration and migration, provided a confined permeation passage for the transport of small molecules, and facilitated quick arrival of reactants to the interface of Cu_xO NPs. While Cu_xO NPs kept high catalytic capability and dispersion inside ZIF-8. Thanks to the desired electrocatalytic activity of Cu_xO NPs and the synergy of the core-shell heterostructure, a satisfactory H_2O_2 sensor was established with a low LOD of 0.15 μM. Another MOFs derivative, α-Fe_2O_3/CNTs, was designed by Jiang's team via in-situ insertion of CNTs into Fe-MOF (MIL-101) and succedent calcination [109]. The MOFs-derived α-Fe_2O_3 polyhedrons adhered closely to the CNTs surface, and hierarchical porous structure was formed on account of the interconnected building blocks. The formed hybrid was further employed as electrode modification material for nitrite detection (Fig. 7b). The incorporation of CNTs shortened the electron transport distance between the α-Fe_2O_3 and CNTs, which endowed α-Fe_2O_3 with high activity for nitrite oxidation. As a result, a desirable sensor for nitrite sensing was built with the LOD down to 0.15 μM. In another work, a MOFs-derived porous carbon (PC) matrix was adopted by Li et al. to load Pt and Co nanoparticles (Pt-Co-PC) for superoxide anions monitoring [110]. Firstly, ZIF-67 was used as MOF precursor for the preparation of Co nanoparticles-porous carbon composite (Co-PC) by one-step carbonization, and then Pt-Co-PC was synthesized via a simple galvanic replacement procedure with Co-PC in $H_2PtCl_6{\cdot}6H_2O$ solution. For one thing, the employment of PC can efficaciously prevent the agglomeration of PtNPs and heighten the stability of Pt-based cat-

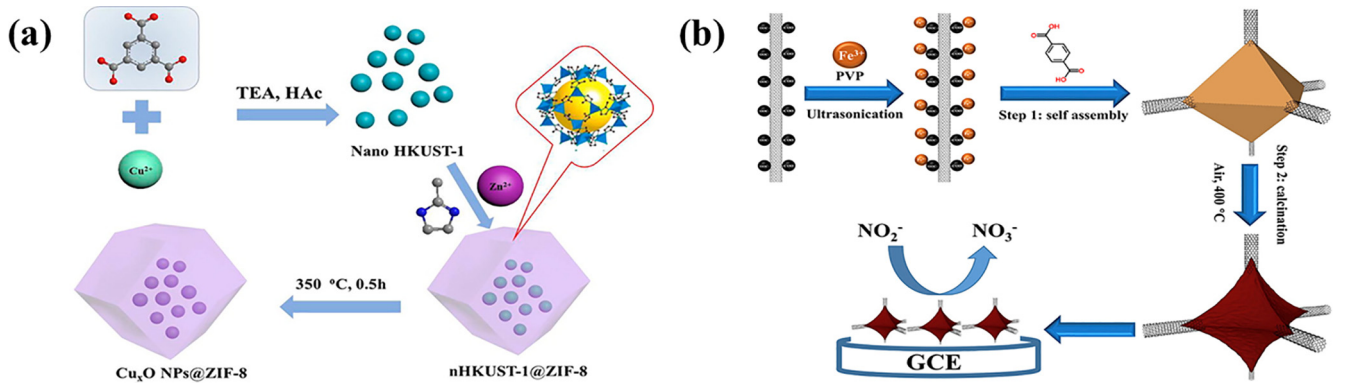

Fig. 7. (a) Schematic diagram of the preparation of Cu_xO NPs@ZIF-8. Adopted from Ref. [108]. Copyright 2016, with permission of American Chemical Society. (b) Schematic illustration of the two-step synthesis routes for MOFs-derived α-Fe_2O_3/CNTs hybrid and its further application for nitrite sensing. Adopted from Ref. [109]. Copyright 2018, with permission of Elsevier.

alyst. For another, an improved electrochemical property was procured in view of the conductivity of PC. Therefore, an enzyme-free sensing platform based on Pt-Co-PC was well fabricated for superoxide anions quantification, with the LOD as low as 0.118 μM. Another example of Pt-based catalyst was proposed by Meng et al. for the determination of methyl parathion (MP) [111]. UiO-66 was utilized simultaneously as a template, ZrO_2 sources, and carbon sources to form ZrO_2 NPs and PCs network. PtNPs were self-immobilized in the surface pores of UiO-66 (Pt/UiO-66). Subsequently, a tri-component nanohybrid of Pt/ZrO_2/PCs was skillfully constructed via direct carbonization of Pt/UiO-66. Profiting from the synergy of high electrochemical activity of PtNPs, remarkable conductivity of PCs, and strong affinity of ZrO_2 for MP, Pt/ZrO_2/PCs exhibited superior performances for MP detection with a low LOD of 1.45×10^{-9} mM. In a recent study, Guo's group prepared a CuCo coated nitrogen-enriched porous carbon polyhedron composite (CuCo@NPCP) for luteolin quantification [112]. The formed CuCo@NPCP possessed the advantages of large specific surface area, distinct 3D porous framework, rich and accessible active sites, and abundant mesoporous structure, which shaped an ideal catalyst for luteolin determination. Therefore, the luteolin sensor based on CuCo@NPCP displayed excellent properties and the LOD was down to 0.08 nM.

4. MOFs and their derivatives as carriers of signal elements

The effective immobilization of signal elements, such as Fc, MB, TMB, and iron(II) phthalocyanine (PcFe), is critical to sensing properties, which is directly related to the LOD, linear range and sensitivity of the sensor [113,114]. The attractive characteristics of MOFs, including large surface area, tunable pore size, high porosity, and multiple functionalization, make it as an ideal carrier for loading signal elements. MOFs can maintain the high redox activity of signal molecules and effectively prevent the leakage of signal molecules, which provides simple, fast, and steady signal output for electrochemical sensing. Besides, the large surface area and porosity of MOFs enable numerous signal molecules to be anchored, which can efficaciously magnify the transduction signal [3].

For instance, Fc was confined in porous Zn-MOF (Fc-Zn-MOF) through post-synthetic modification and further applied by Han et al. as signal tag to amyloid-β (Aβ) determination (Fig. 8a) [115]. High-content Fc was well dispersed in Zn-MOF and stabilized by covalent bonds, exhibiting improved electrochemical activity and good stability. Thus, the highly sensitive and stable electrochemical signal response can be provided by Fc-Zn-MOF in the sensing process. Furthermore, AuNPs-functionalized Fc-Zn-MOF was labeled by detection antibodies (Ab_2-labeled Au@Fc-Zn-MOF). After the sandwich reaction between Ab_2-labeled Au@Fc-Zn-MOF, Aβ, and capture antibodies (Ab_1) immobilized on the electrode surface, a mass of Fc was introduced to the sensing interface, thereby attaining a significant electrochemical signal with LOD of 0.03 pg/mL. Noteworthily, the as-prepared Fc-Zn-MOF still displayed remarkable stability even in extreme acid, alkaline or polar organic solvents. Li et al. proposed a neoteric ratiometric sensor based on MB encased MOF-based nanocomplex for echinacoside (Ech) analysis [116]. Firstly, GO sheets were reduced and modified with NiNPs at the same time, accompanied by mixing with poly (diallydimethylammonium chloride) (PDDA) to form PDDA-rGO-Ni nanocomposite (PGN). Subsequently, Zn-MOF (MOF-5) was grown in situ on PGN, followed by MB encapsulation (MB encased MOF-5@PGN). Then, the as-obtained MB encased MOF-5@PGN was used as a modifier for GCE, and a ratiometric sensor was successfully fabricated based on the electrochemical signal of MB and Ech. Compared with MOF-5@PGN, the incorporation of MB simultaneously widened the linear range ($3.0 \times 10^{-8} - 1.0 \times 10^{-6}$ M), lowered the LOD (1.0×10^{-8} M) and reduced the environmental interference. Such satisfactory electrochemical property was attributed to the synergistic effect of the excellent conductivity of rGO, the superior pore structure of MOF-5, and the unique catalytic ability of NiNPs. In addition, the introduction of MB as a reference signal further boosted the accuracy and sensitivity of detection. In another example, Li's group designed a homogeneous biosensor for early cancer diagnosis by using nucleic acid-functionalized MOFs [117]. UIO-66-NH_2 was selected as nanocarriers to encapsulate electroactive dyes (MB and TMB) and further functionalized by single-stranded DNA C_x (ssDNA C_{MB} and C_{TMB}). Then, double-stranded DNA (dsDNA) was formed as gatekeeper to cap MOFs through the partial hybridization reaction between C_x and another ssDNA P_x (P_{MB} and P_{TMB}). Two functionalized MOFs, containing MB-loaded (MB@UIO) and TMB-loaded nucleic acid-functionalized UIO-66-NH_2 (TMB@UIO), were elaborately constructed and further used for simultaneous determination of multiple tumor biomarkers (let-7a and miRNA-21). The RNA-DNA complexes were formed via the complete hybridization reaction of P_x with target miRNAs, which impelled the RNA-DNA complexes to separate from MOFs, resulting in the release of the electroactive dyes and the strong current signal was obtained (Fig. 8b). In consequence, simultaneous analysis of let-7a and miRNA-21 was realized with the LOD as low as 3.6 fM and 8.2 fM, respectively. In another study, a hierarchically porous MOF@MB connected with aptamer (MOF@MB-Apt) was exploited by He and Dong as signal tag for patulin (PAT) assay [118]. Herein, because of its high specific surface area and chemical stability, ZnO nanoflowers (ZnO NF) were adopted

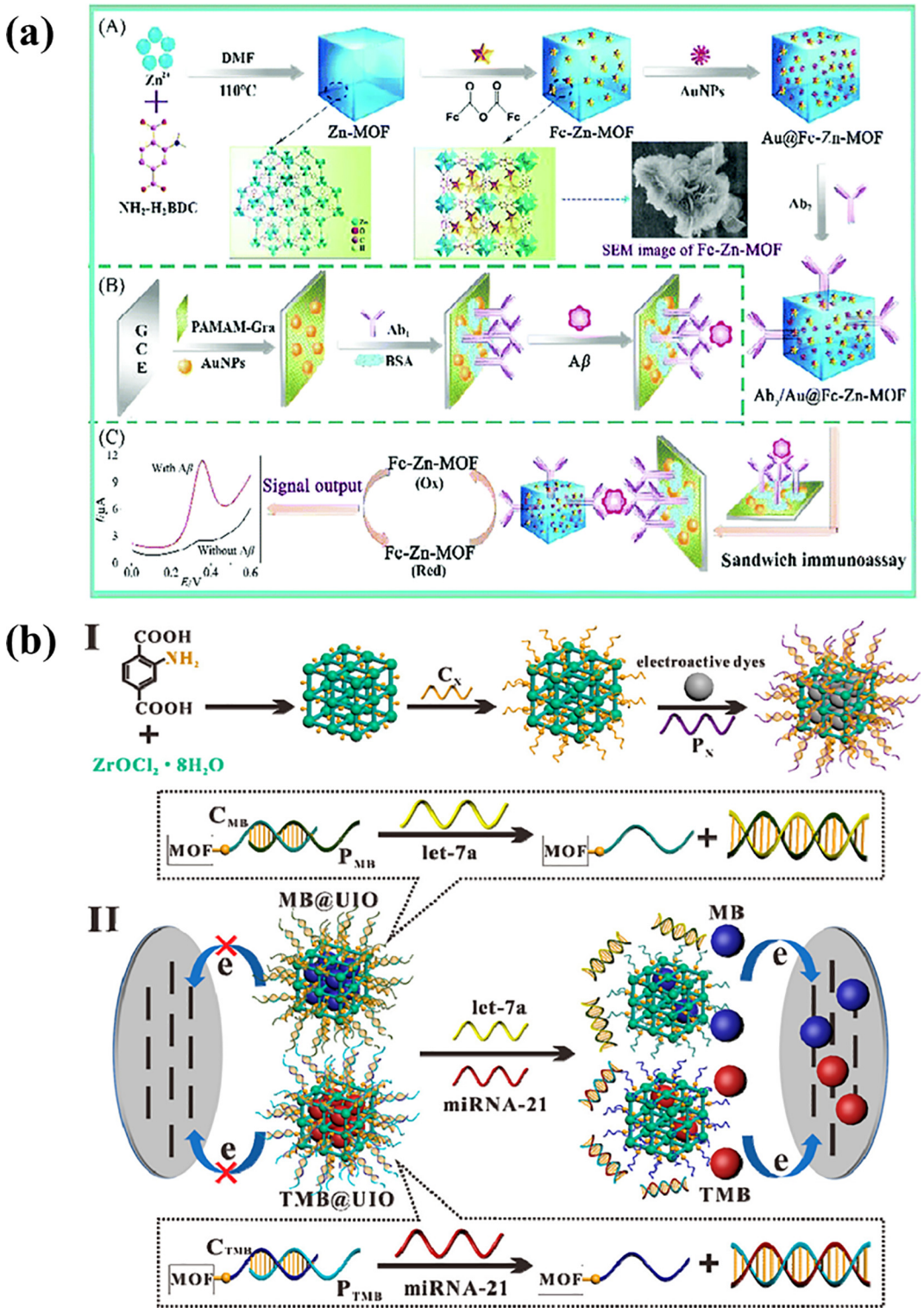

Fig. 8. (a) Schematic illustration of Ab_2/Au@Fc-Zn-MOF fabrication (A), electrochemical immunosensor preparation process (B), and sandwich immunoassay for Aβ detection (C). Adopted from Ref. [115]. Copyright 2017, with permission of Royal Society of Chemistry. (b) Schematic representation of nucleic acid-functionalized MOFs fabrication procedure (I), and the principle of the MOF-based homogeneous electrochemical biosensor for multiple detection of miRNAs (II). Adopted from Ref. [117]. Copyright 2019, with permission of American Chemical Society.

as sensing matrix material and fixed on the gold electrode surface via the adhesion of chitosan (CS), followed by electrodeposition of AuNPs (AuNPs-CS-ZnO) to promote the conductivity. Later, thiol-labeled cDNA (SH-cDNA) was immobilized on the modified electrode surface through Au-S bond. Moreover, the aminated hierarchically porous Zr-MOF (HP-UiO-66-NH_2), with tunable pore size and remarkable encapsulation efficiency, not only provided the desired accessibility for loading MB, but also was easy to link Apt. The obtained MOF@MB-Apt as signal tag was introduced to the electrode surface due to the bonding of Apt and SH-cDNA. After PAT incubation, the signal tags tended to combine with PAT and detach from the electrode surface, leading to a reduced electrochemical signal.

The change of peak current after the addition of PAT was recorded, and the LOD was calculated to be 1.46×10^{-8} μg/mL. In a recent work, Mao's group developed an electrochemical sensor based on PcFe implanted Zn-MOF (PcFe@ZIF-8) for the detection of disinfection by-products (trichloroacetic acid, TCAA) [119]. ZIF-8 had the merits of large surface area, high porosity, good absorbability, unsaturated metal sites, and exceptional chemical stability and flexibility. Meanwhile, PcFe (II) could be converted to PcFe (I) through a reduction process at a given potential. The generated PcFe (I) can be reoxidized by TCAA, resulting in accelerated electron transfer and amplified current signal. ZIF-8 as the carrier of PcFe not only effectively prevented the accumulation and loss of PcFe, but also strengthened the current signal of PcFe thanks to its unsaturated metal sites and high adsorption capacity. Quantitative determination of TCAA was achieved via analyzing the reduction current of PcFe (II), with the LOD as low as 1.89 nM.

5. MOFs and their derivatives as signal probes

Metal ions are usually used as signal tags in electrochemical sensing, displaying specific voltammetric characters at different given potentials [120]. Hence, it provides a viable method for quantitative analysis of target analytes by determining metal components. MOFs are composed of metal ions or clusters bridged by organic ligands, with favorable characteristic of high density of metal sites [121]. Notably, the signal of metal ions in MOFs can be directly measured by electrochemical techniques without acid dissolution and preconcentration, which makes MOFs as simple and convenient signal probes to quantify the concentration of target analytes. The employment of MOFs as signal probes avoids the introduction of foreign signal mediators, simplifying the detection steps and retrenching the detection time. What's more, MOFs contain plentiful metal ions and thus can offer high electrochemical signal [122].

Inspired by this, Liu et al. fabricated an electrochemical immunosensor for the assay of CRP by employing Cu-MOFs (HKUST-1) as signal probes [121]. As shown in Fig. 9a, PtNPs decorated covalent organic frameworks (Pt-COFs) were adopted as matrix material to provide high electronic conductivity and load capture antibodies (Ab_1). Moreover, AuNPs modified Cu-MOFs composite (Au-MOFs), as signal probe, was labeled with signal antibodies (Au-MOFs-Ab_2). In the presence of CRP, signal probes were pulled closer to the electrode surface via antigen–antibody reaction. The electrochemical signal originated from Cu^{2+} reduction was recorded by DPV. Thanks to the abundance of Cu^{2+} in MOFs, the electrochemical signal was largely amplified, and thus a low LOD of 0.2 ng/mL was attained. By taking advantage of Cu-MOFs as signal probes, Wang's team developed a ratiometric electrochemical biosensor based on Cu-trimesic acid MOFs (Cu-BTC MOFs) for monitoring glucose content [123]. Herein, Cu-BTC MOFs

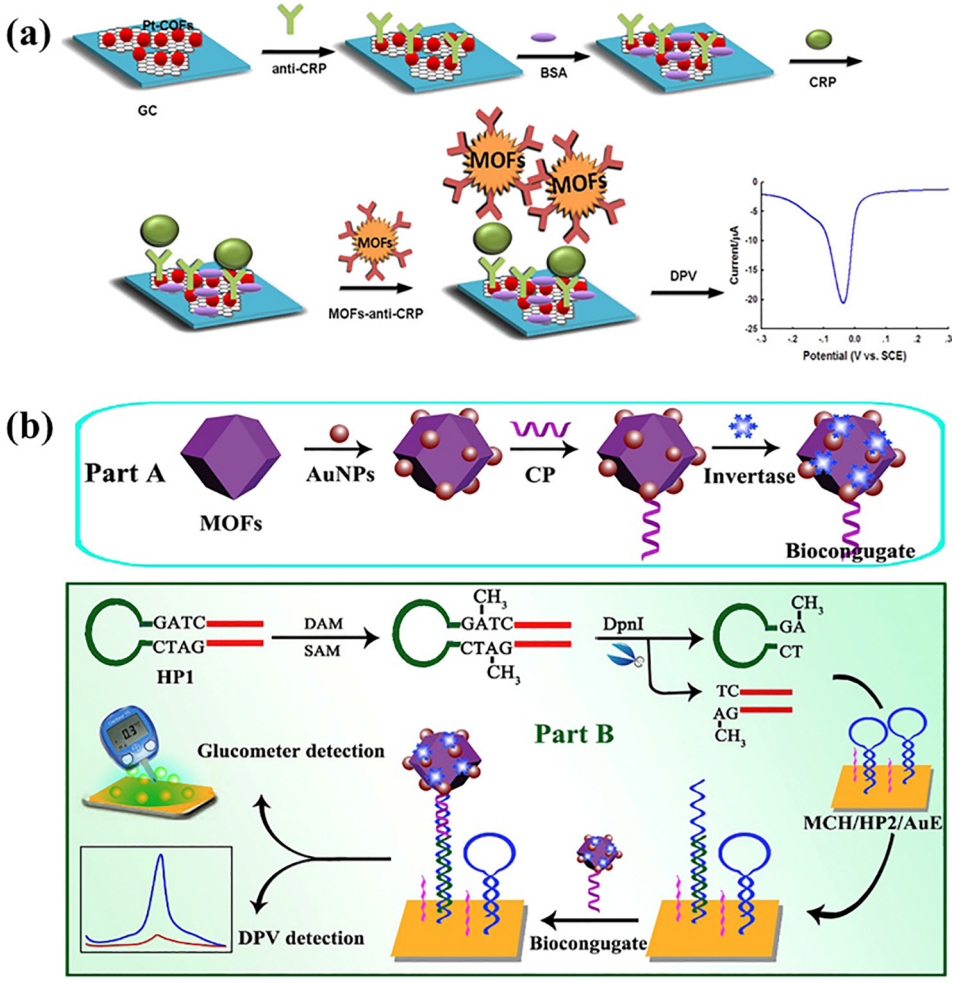

Fig. 9. (a) Schematic illustration of the electrochemical immunosensor for CRP detection. Adopted from Ref. [121]. Copyright 2016, with permission of American Chemical Society. (b) The stepwise preparation of Invertase/CP/Au/CuMOF bioconjugates (A), and schematic illustration of the fabrication process of this proposed dual-response biosensor for Dam MTase activity assay (B). Adopted from Ref. [124]. Copyright 2019, with permission of Elsevier.

were self-assembled on 3D macroporous carbon integrated electrode (3D-KSCs), followed by the electrodeposition of AuNPs with the purpose of catalyzing O_2 reduction, connecting GO_x, and improving the conductivity. Cu-BTC MOFs could catalyze glucose oxidation, and the electrochemical signal of Cu-BTC MOFs was attributed to the redox reaction of Cu. When the glucose concentration was within 4 mM, the reduction peak current of Cu-BTC MOFs increased with the supplementation of glucose, while the reduction peak current of O_2 reduced owing to the O_2 consumption during the catalytic oxidation of glucose by GO_x. In the concentration range of 4 to19 mM, the signal change of Cu-BTC MOFs remained constant because it reached the catalytic limit, while the signal of O_2 still declined. The ratio of O_2 signal to Cu-BTC MOFs signal showed a good linear relationship with glucose concentration, with the LOD of 14.77 μM. Also, Chen et al. designed a dual-response biosensor for monitoring DNA methyltransferase (MTase) activity by using functionalized Cu-MOF as signal probe [124]. AuNPs decorated Cu-MOFs (Au/CuMOFs) simultaneously served as a redox probe for the generation of electrochemical signals and a support platform for the fixation of invertase. As shown in Fig. 9b, the bioconjugates (Invertase/CP/Au/CuMOFs) were formed by connecting Au/CuMOFs with capture probe (CP) and invertase. After the addition of Dam MTase, hairpin probe 1 (HP1) was methylated and subsequently cleaved with the aid of a restriction endonuclease (DpnI), and thus a binding sequence was released to hybridize with hairpin probe 2 (HP2) immobilized on the electrode surface. Then, the hairpin structure of HP2 was opened and the sticky terminus was exposed to further react with CP, therefore Invertase/CP/Au/CuMOFs was attached to the electrode surface. At last, glucose was produced by the catalysis of invertase after incubating the modified electrode in sucrose solution. For dual-response signal output, the current response of Cu^{2+} in Cu-MOFs was monitored by DPV and the incubation buffer was measured by a commercial glucometer, with the LOD of 0.001 and 0.007 U/mL, respectively. In another study, Yang et al. constructed an electrochemical aptasensor for Tb analysis based on PtPd NPs loaded Co-MOFs (Co-MOFs/PtPdNPs) as redox mediator and a modified target-triggering nicking enzyme signaling amplification (NESA) tactic as signal amplifier [125]. On the one hand, the improved NESA tactic could avoid the waste of DNA strands and achieve efficient utilization of output DNA. On the other hand, the electroactive Co-MOFs not only acted as signal tags, but also served as nanocarrier to load PtPd NPs. The incorporated PtPd NPs could catalyze the oxidation of H_2O_2, accelerating the transformation of Co^{2+} into Co^{3+}. Benefiting from such design, the electrochemical signal was greatly amplified with the LOD down to 0.32 pM. In a recent study, Liu et al. proposed an electrochemical immunoassay by the employment of Ag-MOFs as a signal probe for CEA detection [122]. The electrochemical signal of Ag(I) in Ag-MOFs could be directly detected and was relatively stable, which made Ag-MOFs as feasible signal probes. Herein, Ag-MOFs played a significant role in two aspects. For one thing, Ag-MOFs as nanocarriers were modified by AuNPs to immobilize anti-CEA. For another, the electroactive Ag-MOFs, as signal probes, were captured on the electrode surface via antigen–antibody binding for signal generation. The electrochemical signal from the redox response of Ag-MOFs was monitored by DPV, and the peak current of DPV had a good linear correlation with CEA concentration, with the LOD of 8.0 fg/mL.

6. MOFs and their derivatives as concentrators

Heavy metal ions, even at trace levels, pose a severe threat to human health and the natural environment on account of their high toxicity, good stability, and easy accumulation through the food chain [126]. Therefore, the development of a simple, sensitive, and reliable detection technology for the assay of trace heavy metal ions is still highly in demand [127].

Thanks to the merits of simplicity, portability, high sensitivity, cost effectiveness, and simultaneous multielement analysis, anodic stripping voltammetry (ASV) has been recognized a potent analytical technique for the determination of trace heavy metal ions [128]. Notably, the ultra-high sensitivity of ASV is ascribable to the combination of effective preconcentration steps and advanced measurement procedures, which produces a fairly favorable signal-to-background ratio [129]. ASV measurement normally involves two processes: the electrolytic enrichment of analytes and electrochemical stripping of the enriched analytes. The location and peak current of stripping peak are utilized to identify and quantify the analytes, respectively [130]. Since the electrochemical processes occur on the working electrode surface, the appropriate selection of the working electrode is essential to realize highly sensitive detection. MOFs offer the characteristics of large surface area, high porosity, adjustable pore sizes, and tunable chemical functionality. The use of MOFs as electrode modifier is a decent choice to promote the performance of working electrodes. MOFs are used here as concentrators to improve the preconcentration process of ASV measurement, further enlarging the detection sensitivity and causing a signal amplification. By the combination of MOFs as concentrators and ASV, Wang et al. synthesized a Zn-MOF (MOF-5) to modify carbon paste electrode (CPE) for Pb^{2+} sensing [131]. The results demonstrated that MOF-5 was able to selectively adsorb Pb^{2+} from aqueous solutions, which facilitated the preconcentration of Pb^{2+} at the modified electrode surface. After the chemical accumulation of Pb^{2+}, the electrochemical determination of the enriched analytes was performed by differential pulse anodic stripping voltammetry (DPASV) with the LOD down to 4.9×10^{-9} M. In another study, Guo's group prepared a cauliflower-like Cr-MOF (MIL-100(Cr)) via a facile reflux method for simultaneous determination of multiple heavy metal ions [132]. The MIL-100(Cr)/GCE as working electrode was propitious to the enrichment process of Cd^{2+}, Pb^{2+}, Cu^{2+}, and Hg^{2+}, and the carboxyl group was speculated to be anchor sites for the adsorption of heavy metal ions. Cd^{2+}, Pb^{2+}, Cu^{2+}, and Hg^{2+} can be identified at different potentials and quantified by square wave anodic stripping voltammetry (SWASV) with the LOD of 4.4×10^{-8} M, 4.8×10^{-8} M, 1.1×10^{-8} M, 8.8×10^{-9} M, respectively. Furthermore, Guo's group also fabricated a nanoscale amino-functionalized Ni-MOF through a one-pot hydrothermal treatment for Pb^{2+} assay [133]. Pb^{2+} could be adsorbed by the amino group on the Ni-MOF surface, and the ion size exclusion effect of Ni-MOF further boosted the selectivity. Subsequently, the electrochemical detection of Pb^{2+} was conducted by SWASV with a LOD of 5.08×10^{-7} M. In another example, Wang's team first developed an anionic MOF (Me_2NH_2@MOF-1) for Cu^{2+} quantification [134]. Moreover, AuNPs as a binder enhanced the electrochemical signal and promoted the sensitivity by ion exchange. The composite of Me_2NH_2@MOF-1 and AuNPs exhibited high sensitivity to Cu^{2+}, which could be attributed to the 3D structure and cationic exchange of Me_2NH_2@MOF-1, as well as the synergistic effect of AuNPs. The 3D structure of Me_2NH_2@MOF-1 provided a high active surface area, meanwhile, Me_2NH_2@MOF-1 acted as a pre-concentrator through the cationic exchange of $[H_2N(CH_3)_2]^+$ with Cu^{2+}. With such a design, the SWASV signal of Cu^{2+} was greatly amplified with the LOD as low as 1×10^{-12} M. In a recent work, Shi et al. prepared a metal Bi encapsulated MIL-101(Cr) (Bi/MIL-101(Cr)) by electrochemical reduction of Bi (III)-impregnated MIL-101(Cr) for the simultaneous analysis of Cd^{2+} and Pb^{2+} (Fig. 10) [135]. Compared to the single-component counterparts, the Bi/MIL-101(Cr)/GCE displayed an obviously rising DPASV peak current, which was primarily derived from the rich pore structure of MIL-101(Cr), the selective formation of target metal–ligand complex together with the catalytic activity of

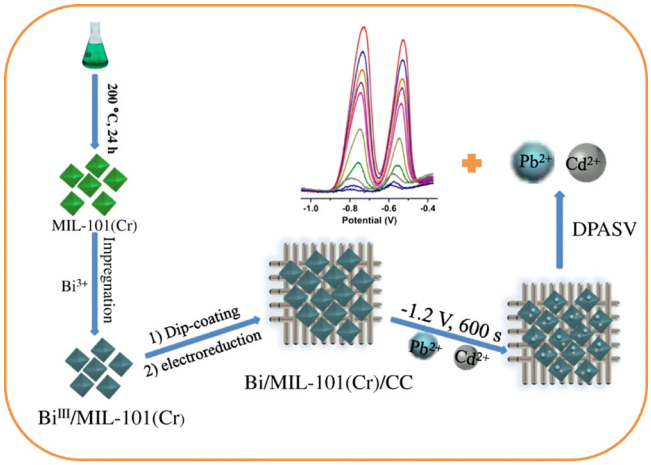

Fig. 10. Schematic illustration for the synthesis of Bi/MIL-101(Cr)/GCE composite, and its application for electrochemical detection of Cd^{2+} and Pb^{2+}. Adopted from Ref. [135]. Copyright 2019, with permission of Springer.

MIL-101(Cr) and Bi. On this basis, a sensor with impressive performance for Cd^{2+} and Pb^{2+} detection was successfully constructed with the LOD of 0.06 μg/L and 0.07 μg/L, respectively. In addition, Xiao et al. employed a MOF derivative as the sensing platform in combination with DPASV for the measurement of Cd^{2+} and Pb^{2+} [136]. A nitrogen doped microporous carbon (NMC) composite was attained by the direct carbonization of ZIF-8. The resultant NMC, with a larger effective surface area, supplied more active sites for metal ions adsorption, and the high nitrogen doping content of NMC availed the accumulation of target metal ions owing to its favorable affinity to heavy metal ions. Besides, the good conductivity of NMC stemmed from the 3D carbon network and nitrogen doping facilitated the charge transport. All these properties of NMC contributed to electrochemical activity. Also, Nafion and Bi film were introduced to boost the stripping signals. Profiting from the synergistic effect, the LODs of 1.5 μg/L for Cd^{2+} and 0.05 μg/L for Pb^{2+} were achieved.

As another voltammetry technique, DPV is also a common strategy for the quantitative analysis of heavy metal ions. The advantageous signal-to-noise ratio provided by DPV leads to a favorable detection sensitivity. Roushani and his colleagues built an amino-functionalized Zn-MOF (TMU-16-NH_2) modified CPE for Cd^{2+} sensing [137]. TMU-16-NH_2 possessed high porosity and amine groups could selectively bind to Cd^{2+} through Cd^{2+}-N complexation, which made for the adsorption of Cd^{2+} and further enhanced the sensitivity of assay. Under optimal conditions, DPV was applied to quantify Cd^{2+} and a low LOD of 0.2 μg/L was obtained. Similarly, Wang et al. fabricated a conductive electrochemical sensor for Cd^{2+} determination based on polyaniline (PANI) loaded Zr-MOF (UiO-66-NH_2@PANI) [138]. PANI was polymerized on the surface of UiO-66-NH_2 to promote the conductivity by expediting electron/ion diffusion. UiO-66-NH_2 not only acted as a scaffold for PANI loading, but also offered a large surface area and abundant amine groups for target analyte adsorption. Thus, a reliable detection of Cd^{2+} was implemented by DPV thanks to the chelation mechanism between Cd^{2+} and amino, with the LOD down to 0.3 μg/L.

7. Conclusions and perspectives

As a rapidly developing field, MOF-based electrochemical sensors have acquired fruitful achievements. MOFs possess numerous intriguing characteristics, including larger surface area, high porosity, unsaturated metal sites, adjustable pore size and chemical functionality, which enable MOFs and their derivatives to be effectively utilized for signal amplification in electrochemical sensing. In this review, we have summarized the recent developments of MOFs and their derivatives as electrochemical signal amplification elements and divided the signal amplification routes into five categories according to their disparate role in electrochemical sensors. Firstly, MOFs and their derivatives can act as support platforms for the immobilization of biomolecules with target recognition functions, such as antibodies and aptamers. More biomolecules can be stably fixed on MOFs and their derivatives to further heighten the signal. Secondly, partial MOFs hold inherent enzyme-mimicking catalytic activity, which makes them as stable catalysts to replace natural enzymes, boosting the sensitivity of electrochemical sensors. Besides, the catalytic performance of MOFs can be greatly promoted through some modification means, further amplifying the signal. Thirdly, MOFs and their derivatives, as carriers of signal elements, could effectively prevent the leakage of signal molecules and keep their high redox activity, together with providing high surface area and porosity to anchor numerous signal molecules, thus efficaciously magnifying the transduction signal. Fourthly, metal ions in MOFs can be directly detected by electrochemical techniques, which suggests MOFs as simple and convenient signal probes for electrochemical sensing. Abundant metal ions in MOFs offer high electrochemical signal for detection. Finally, MOFs and their derivatives can combine with voltammetry technique for the determination of heavy metal ions. Here, MOFs and their derivatives serve as concentrators to improve the preconcentration process of voltammetry measurement, which enlarges the detection sensitivity and causes a signal amplification. In addition, MOFs and their derivatives can perform multiple functions at the same time, such as acting as catalysts, signal probes and carriers simultaneously. In summary, the various properties of MOFs and their derivatives enable them to exert different roles in electrochemical sensing, and ultimately achieve the purpose of signal amplification.

However, many challenges remain for the application of MOFs and their derivatives as signal amplification elements in electrochemical sensing. (1) Non-specific adsorption of coexisting substances would occur in complex matrix owing to the large surface area of MOFs, which has a negative impact on the sensing performance. Fine regulation of pore structure of MOFs can provide precision for selective adsorption of target analytes, offering a feasible method to break through the above barrier. (2) Weak material properties cause most MOFs to be unstable in aqueous media. Surface modification is a good solution to improve the stability of MOFs in water, such as modifying hydrophobic materials or functional groups on the surface of MOFs. (3) MOFs and their derivatives as peroxidase-like catalysts have much lower catalytic activity than natural enzymes. The construction of 2D MOFs and their derivatives with higher surface area and richer active sites can alleviate this problem to some extent. Moreover, reasonable selection of multivalent ligands and metal nodes can also enhance the catalytic activity of MOFs. (4) The weak binding force between target analytes and MOFs and their derivatives can affect the sensitivity of detection. Surface functional group modification is a decent choice to supply more firm binding sites for the adsorption of target analytes. (5) The conductivity of most MOFs is unsatisfactory. In addition to the carbonization of MOFs and the introduction of high conductivity species into the host MOFs, in-situ or post-treatment doping of conductive impurities into MOFs is also an alternative to enhance the conductivity. To date, electrochemical sensing based on MOFs and their derivatives is still limited under laboratory conditions. Ongoing efforts on MOFs and their derivatives need to be done to pave the avenue for further applications. Nevertheless, in view of the unparalleled characteristics of MOFs, we are convinced that with the development of nanoscience and biotechnology, MOF-based electrochemical sensors will bring a

bright future to routine biomedical, clinical, and environmental analysis.

Declaration of Competing Interest

The authors declare that they have no known competing financial interests or personal relationships that could have appeared to influence the work reported in this paper.

Acknowledgements

This study was financially supported by the Program for the National Natural Science Foundation of China (51879101, 51579098, 51809090, 51779090, 51709101, 51521006, 51909084), the National Program for Support of Top-Notch Young Professionals of China (2014), the Program for Changjiang Scholars and Innovative Research Team in University (IRT-13R17), and Hunan Provincial Science and Technology Plan Project (2018SK20410, 2017SK2243, 2016RS3026), and the Fundamental Research Funds for the Central Universities (531119200086, 531118010114, 531107050978, 541109060031).

References

[1] X. Zhang, G. Li, D. Wu, X. Li, N. Hu, J. Chen, G. Chen, Y. Wu, Biosens. Bioelectron. 137 (2019) 178–198.
[2] Y. Li, Z. Wang, L. Sun, L. Liu, C. Xu, H. Kuang, TrAC, Trends Anal. Chem. 113 (2019) 74–83.
[3] L. Wu, E. Xiong, X. Zhang, X. Zhang, J. Chen, Nano Today 9 (2014) 197–211.
[4] C. Lai, S. Liu, C. Zhang, G. Zeng, D. Huang, L. Qin, X. Liu, H. Yi, R. Wang, F. Huang, B. Li, T. Hu, ACS Sens. 3 (2018) 2566–2573.
[5] G. Zeng, C. Zhang, D. Huang, C. Lai, L. Tang, Y. Zhou, P. Xu, H. Wang, L. Qin, M. Cheng, Biosens. Bioelectron. 90 (2016) 542–548.
[6] X. Liu, D. Huang, C. Lai, G. Zeng, L. Qin, C. Zhang, H. Yi, B. Li, R. Deng, S. Liu, Y. Zhang, TrAC, Trends Anal. Chem. 109 (2018) 260–274.
[7] X. Fang, B. Zong, S. Mao, Nano-Micro Lett. 10 (2018) 64.
[8] R. Abolhasan, A. Mehdizadeh, M.R. Rashidi, L. Aghebati-Maleki, M. Yousefi, Biosens. Bioelectron. 129 (2019) 164–174.
[9] C. Zhang, C. Lai, G. Zeng, D. Huang, L. Tang, C. Yang, Y. Zhou, L. Qin, M. Cheng, Biosens. Bioelectron. 81 (2016) 61–67.
[10] Y. Zhang, G.M. Zeng, L. Tang, J. Chen, Y. Zhu, X.X. He, Y. He, Anal. Chem. 87 (2015) 989–996.
[11] M. Zhou, L. Shang, B. Li, L. Huang, S. Dong, Biosens. Bioelectron. 24 (2008) 442–447.
[12] Z. Xue, F. Zhang, D. Qin, Y. Wang, J. Zhang, J. Liu, Y. Feng, X. Lu, Carbon 69 (2014) 481–489.
[13] C. Zhang, W. Wang, A. Duan, G. Zeng, D. Huang, C. Lai, X. Tan, M. Cheng, R. Wang, C. Zhou, W. Xiong, Y. Yang, Chemosphere 222 (2019) 184–194.
[14] D. Chen, X. Zhuang, J. Zhai, Y. Zheng, H. Lu, L. Chen, Sens. Actuators, B 255 (2018) 1500–1506.
[15] L. Cheng, X. Liu, J. Lei, H. Ju, Anal. Chem. 82 (2010) 3359–3364.
[16] J. Cha, J.I. Han, Y. Choi, D.S. Yoon, K.W. Oh, G. Lim, Biosens. Bioelectron. 18 (2003) 1241–1247.
[17] X. Huo, P. Liu, J. Zhu, X. Liu, H. Ju, Biosens. Bioelectron. 85 (2016) 698–706.
[18] S. Liu, J. Zhang, W. Tu, J. Bao, Z. Dai, Nanoscale 6 (2014) 2419–2425.
[19] D. He, C. Zhang, G. Zeng, Y. Yang, D. Huang, L. Wang, H. Wang, Appl. Catal. B Environ. 258 (2019) 117957.
[20] Y. Zhang, S. Yuan, G. Day, X. Wang, X. Yang, H.C. Zhou, Coordin. Chem. Rev. 354 (2018) 28–45.
[21] S. Carrasco, Biosensors 8 (2018) 92.
[22] Q. Wang, X. Lian, Y. Fang, H.C. Zhou, Catalysts 8 (2018) 166.
[23] F.Y. Yi, D. Chen, M.K. Wu, L. Han, H.L. Jiang, Chempluschem 81 (2016) 675–690.
[24] L.T. Liu, Y.L. Zhou, S. Liu, M.T. Xu, ChemElectroChem 5 (2018) 6–19.
[25] Q.L. Zhu, Q. Xu, Chem. Soc. Rev. 43 (2014) 5468–5512.
[26] Z. Hu, B.J. Deibert, J. Li, Chem. Soc. Rev. 43 (2014) 5815–5840.
[27] J. Lei, R. Qian, P. Ling, L. Cui, H. Ju, TrAC, Trends Anal. Chem. 58 (2014) 71–78.
[28] S. Li, X. Liu, H. Chai, Y. Huang, TrAC, Trends Anal. Chem. 105 (2018) 391–403.
[29] W.P. Lustig, S. Mukherjee, N.D. Rudd, A.V. Desai, J. Li, S.K. Ghosh, Chem. Soc. Rev. 46 (2017) 3242–3285.
[30] A. Morozan, F. Jaouen, Energy Environ. Sci. 5 (2012) 9269.
[31] C.S. Liu, J.J. Li, H. Pang, Coordin. Chem. Rev. 410 (2020) 213222.
[32] S. Kempahanumakkagari, K. Vellingiri, A. Deep, E.E. Kwon, N. Bolan, K.H. Kim, Coordin. Chem. Rev. 357 (2018) 105–129.
[33] F. Zhao, T. Sun, F.Y. Geng, P.Y. Chen, Y.P. Guo, Int. J. Electrochem. Sci. 14 (2019) 5287–5304.
[34] C.S. Liu, C.X. Sun, J.Y. Tian, Z.W. Wang, H.F. Ji, Y.P. Song, S. Zhang, Z.H. Zhang, L. H. He, M. Du, Biosens. Bioelectron. 91 (2017) 804–810.
[35] Z. Tang, J. He, J. Chen, Y. Niu, Y. Zhao, Y. Zhang, C. Yu, Biosens. Bioelectron. 101 (2018) 253–259.
[36] W. Xu, Z. Qin, Y. Hao, Q. He, S. Chen, Z. Zhang, D. Peng, H. Wen, J. Chen, J. Qiu, C. Li, Biosens. Bioelectron. 113 (2018) 148–156.
[37] M. Hu, X. Hu, Y. Zhang, M. Teng, R. Deng, G. Xing, J. Tao, G. Xu, J. Chen, Y. Zhang, G. Zhang, Sens. Actuat. B 288 (2019) 571–578.
[38] H.M. Meng, H. Liu, H. Kuai, R. Peng, L. Mo, X.B. Zhang, Chem. Soc. Rev. 45 (2016) 2583–2602.
[39] A.B. Iliuk, L. Hu, W.A. Tao, Anal. Chem. 83 (2011) 4440–4452.
[40] C.S. Liu, Z.H. Zhang, M. Chen, H. Zhao, F.H. Duan, D.M. Chen, M.H. Wang, S. Zhang, M. Du, Chem. Commun. 53 (2017) 3941–3944.
[41] F. Su, S. Zhang, H. Ji, H. Zhao, J.Y. Tian, C.S. Liu, Z. Zhang, S. Fang, X. Zhu, M. Du, ACS Sens. 2 (2017) 998–1005.
[42] Z.H. Zhang, F.H. Duan, J.Y. Tian, J.Y. He, L.Y. Yang, H. Zhao, S. Zhang, C.S. Liu, L. H. He, M. Chen, D.M. Chen, M. Du, ACS Sens. 2 (2017) 982–989.
[43] C. Zhang, J. He, Y. Zhang, J. Chen, Y. Zhao, Y. Niu, C. Yu, Biosens. Bioelectron. 102 (2018) 94–100.
[44] Y. Chen, X. Liu, S. Guo, J. Cao, J. Zhou, J. Zuo, L. Bai, Biomaterials 216 (2019) 119253.
[45] N. Zhou, F. Su, C. Guo, L. He, Z. Jia, M. Wang, Q. Jia, Z. Zhang, S. Lu, Biosens. Bioelectron. 123 (2019) 51–58.
[46] Z. Jia, Y. Ma, L. Yang, C. Guo, N. Zhou, M. Wang, L. He, Z. Zhang, Biosens. Bioelectron. 133 (2019) 55–63.
[47] H. Yi, M. Yan, D. Huang, G. Zeng, C. Lai, M. Li, X. Huo, L. Qin, S. Liu, X. Liu, B. Li, H. Wang, M. Shen, Y. Fu, X. Guo, Appl. Catal. B Environ. 250 (2019) 52–62.
[48] H. Wei, E. Wang, Chem. Soc. Rev. 42 (2013) 6060.
[49] X. Liu, D. Huang, C. Lai, L. Qin, G. Zeng, P. Xu, B. Li, H. Yi, M. Zhang, Small 15 (2019) 1900133.
[50] J. Liu, X. Bo, J. Yang, D. Yin, L. Guo, Sens. Actuat. B 248 (2017) 207–213.
[51] Y.Z. Chen, R. Zhang, L. Jiao, H.L. Jiang, Coordin. Chem. Rev. 362 (2018) 1–23.
[52] Y. Wang, M. Zhao, J. Ping, B. Chen, X. Cao, Y. Huang, C. Tan, Q. Ma, S. Wu, Y. Yu, Q. Lu, J. Chen, W. Zhao, Y. Ying, H. Zhang, Adv. Mater. 28 (2016) 4149–4155.
[53] N.S. Lopa, M.M. Rahman, F. Ahmed, S. Chandra Sutradhar, T. Ryu, W. Kim, Electrochim. Acta 274 (2018) 49–56.
[54] W. Ling, G. Liew, Y. Li, Y. Hao, H. Pan, H. Wang, B. Ning, H. Xu, X. Huang, Adv. Mater. 30 (2018) 1800917.
[55] S. Dong, G. Suo, N. Li, Z. Chen, L. Peng, Y. Fu, Q. Yang, T. Huang, Sens. Actuat. B 222 (2016) 972–979.
[56] P. Ling, J. Lei, L. Jia, H. Ju, Chem. Commun. 52 (2016) 1226–1229.
[57] Z. Wang, H. Yu, J. Han, G. Xie, S. Chen, Chem. Commun. 53 (2017) 9926–9929.
[58] Z. Wang, P. Dong, Z. Sun, C. Sun, H. Bu, J. Han, S. Chen, G. Xie, J. Mater. Chem. B 6 (2018) 2426–2431.
[59] L. Qin, Z. Zeng, G. Zeng, C. Lai, A. Duan, R. Xiao, D. Huang, Y. Fu, H. Yi, B. Li, X. Liu, S. Liu, M. Zhang, D. Jiang, Appl. Catal. B Environ. 259 (2019) 118035.
[60] J. He, C. Lai, L. Qin, B. Li, S. Liu, L. Jiao, Y. Fu, D. Huang, L. Li, M. Zhang, X. Liu, H. Yi, L. Chen, Z. Li, Chemosphere 256 (2020) 127083.
[61] Q. Yang, Q. Xu, H.L. Jiang, Chem. Soc. Rev. 46 (2017) 4774–4808.
[62] L. Qin, D. Huang, P. Xu, G. Zeng, C. Lai, Y. Fu, H. Yi, B. Li, C. Zhang, M. Cheng, C. Zhou, X. Wen, J. Colloid Interf. Sci. 534 (2019) 357–369.
[63] Y. Fu, L. Qin, D. Huang, G. Zeng, C. Lai, B. Li, J. He, H. Yi, M. Zhang, M. Cheng, X. Wen, Appl. Catal. B Environ. 255 (2019) 117740.
[64] W.J. Shen, Y. Zhuo, Y.Q. Chai, R. Yuan, Anal. Chem. 87 (2015) 11345–11352.
[65] W.J. Shen, Y. Zhuo, Y.Q. Chai, R. Yuan, Biosens. Bioelectron. 83 (2016) 287–292.
[66] H. Yu, J. Han, S. An, G. Xie, S. Chen, Biosens. Bioelectron. 109 (2018) 63–69.
[67] P. Dong, L. Zhu, J. Huang, J. Ren, J. Lei, Biosens. Bioelectron. 138 (2019) 111313.
[68] Z. Xu, L. Yang, C. Xu, Anal. Chem. 87 (2015) 3438–3444.
[69] Y. Li, C. Yu, B. Yang, Z. Liu, P. Xia, Q. Wang, Biosens. Bioelectron. 102 (2018) 307–315.
[70] C. Li, R. Wu, J. Zou, T. Zhang, S. Zhang, Z. Zhang, X. Hu, Y. Yan, X. Ling, Biosens. Bioelectron. 116 (2018) 81–88.
[71] Q. Liu, J.S. Dordick, C.Z. Dinu, ACS Appl. Mater. Inter. 11 (2019) 31049–31059.
[72] C. Lai, M. Zhang, B. Li, D. Huang, G. Zeng, L. Qin, X. Liu, H. Yi, M. Cheng, L. Li, Z. Chen, L. Chen, Chem. Eng. J. 358 (2019) 891–902.
[73] B. Li, S. Liu, C. Lai, G. Zeng, M. Zhang, M. Zhou, D. Huang, L. Qin, X. Liu, Z. Li, N. An, F. Xu, H. Yi, Y. Zhang, L. Chen, Appl. Catal. B Environ. 266 (2020) 118650.
[74] X. Zhou, C. Lai, D. Huang, G. Zeng, L. Chen, L. Qin, P. Xu, M. Cheng, C. Huang, C. Zhang, C. Zhou, J. Hazard. Mater 346 (2018) 113–123.
[75] Q. Wang, X. Zhang, L. Huang, Z. Zhang, S. Dong, Angew. Chem. Int. Ed. 56 (2017) 16082–16085.
[76] Y. Yu, C. Yu, Y. Niu, J. Chen, Y. Zhao, Y. Zhang, R. Gao, J. He, Biosens. Bioelectron. 101 (2018) 297–303.
[77] H. Hosseini, H. Ahmar, A. Dehghani, A. Bagheri, A.R. Fakhari, M.M. Amini, Electrochim. Acta 88 (2013) 301–309.
[78] W. Yang, W. Lu, C. Huanhuan, H. Xiaoya, M. Shengqian, ACS Appl. Mater. Inter. 8 (2016) 18173–18181.
[79] H. Wang, Y. Jian, Q. Kong, H. Liu, F. Lan, L. Liang, S. Ge, J. Yu, Sens. Actuat. B 257 (2018) 561–569.
[80] H. Dong, X. Hu, J. Zhao, H. Li, K. Koh, L. Gao, M. Shao, H. Chen, Sens. Actuat. B 276 (2018) 150–157.
[81] H. Chen, T. Yang, F. Liu, W. Li, Sens. Actuat. B 286 (2019) 401–407.
[82] Y. Dong, C. Duan, Q. Sheng, J. Zheng, Analyst 144 (2019) 521–529.
[83] B. Reuillard, S. Gentil, M. Carriere, A. Le Goff, S. Cosnier, Chem. Sci. 6 (2015) 5139–5143.

[84] L. Wang, H. Yang, J. He, Y. Zhang, J. Yu, Y. Song, Electrochim. Acta 213 (2016) 691–697.
[85] M. Zhang, Z.Y. Gu, M. Bosch, Z. Perry, H.C. Zhou, Coordin. Chem. Rev. 293–294 (2015) 327–356.
[86] S. Xie, J. Ye, Y. Yuan, Y. Chai, R. Yuan, Nanoscale 7 (2015) 18232–18238.
[87] J. Chen, C. Yu, Y. Zhao, Y. Niu, L. Zhang, Y. Yu, J. Wu, J. He, Biosens. Bioelectron. 91 (2017) 892–899.
[88] L. Wang, Q. Teng, X. Sun, Y. Chen, Y. Wang, H. Wang, Y. Zhang, J. Colloid Interf. Sci. 512 (2018) 127–133.
[89] X. Zhou, Z. Zeng, G. Zeng, C. Lai, R. Xiao, S. Liu, D. Huang, L. Qin, X. Liu, B. Li, H. Yi, Y. Fu, L. Li, Z. Wang, Chem. Eng. J. 383 (2020) 123091.
[90] C. Lai, F. Huang, G. Zeng, D. Huang, L. Qin, M. Cheng, C. Zhang, B. Li, H. Yi, S. Liu, L. Li, L. Chen, Chemosphere 224 (2019) 910–921.
[91] L. Li, C. Lai, F. Huang, M. Cheng, G. Zeng, D. Huang, B. Li, S. Liu, M. Zhang, L. Qin, M. Li, J. He, Y. Zhang, L. Chen, Water Res. 160 (2019) 238–248.
[92] Y. Zhang, P. Yan, Q. Wan, N. Yang, Carbon 134 (2018) 540–547.
[93] B. Li, C. Lai, G. Zeng, D. Huang, L. Qin, M. Zhang, M. Cheng, X. Liu, H. Yi, C. Zhou, F. Huang, S. Liu, Y. Fu, Small 15 (2019) 1804565.
[94] Y.Y. Wang, C. Hou, Y. Zhang, F. He, M. Liu, X. Li, J. Mater. Chem. B 4 (2016) 3695–3702.
[95] X. Chen, D. Liu, G. Cao, Y. Tang, C. Wu, ACS Appl. Mater. Inter. 11 (2019) 9374–9384.
[96] X. Li, C. Li, C. Wu, K. Wu, Anal. Chem. 91 (2019) 6043–6050.
[97] Y. Xie, X. Tu, X. Ma, M. Xiao, G. Liu, F. Qu, R. Dai, L. Lu, W. Wang, Electrochim. Acta 311 (2019) 114–122.
[98] S. Liu, C. Lai, B. Li, C. Zhang, M. Zhang, D. Huang, L. Qin, H. Yi, X. Liu, F. Huang, X. Zhou, L. Chen, Chem. Eng. J. 384 (2020) 123304.
[99] M.Q. Wang, Y. Zhang, S.J. Bao, Y.N. Yu, C. Ye, Electrochim. Acta 190 (2016) 365–370.
[100] W. Bai, S. Li, J. Ma, W. Cao, J. Zheng, J. Mater. Chem. A 7 (2019) 9086–9098.
[101] W. Meng, S. Xu, L. Dai, Y. Li, J. Zhu, L. Wang, Electrochim. Acta 230 (2017) 324–332.
[102] Y. Chen, X. Sun, S. Biswas, Y. Xie, Y. Wang, X. Hu, Biosens. Bioelectron. 141 (2019) 111470.
[103] Y. Chen, W. Huang, K. Chen, T. Zhang, Y. Wang, J. Wang, Sens. Actuat. B 290 (2019) 434–442.
[104] X. Wang, X. Lu, L. Wu, J. Chen, Biosens. Bioelectron. 65 (2015) 295–301.
[105] X. Lu, X. Wang, L. Wu, L. Wu, L. Dhanjai, Y. Fu, J.C. Gao, ACS Appl. Mater. Inter. 8 (2016) 16533–16539.
[106] C. Zhang, X. Wang, M. Hou, X. Li, X. Wu, J. Ge, ACS Appl. Mater. Inter. 9 (2017) 13831–13836.
[107] H.B. Wu, X.W. Lou, Sci. Adv. 3 (2017) eaap9252.
[108] J. Yang, H. Ye, F. Zhao, B. Zeng, ACS Appl. Mater. Inter. 8 (2016) 20407–20414.
[109] K. Wang, C. Wu, F. Wang, C. Liu, C. Yu, G. Jiang, Electrochim. Acta 285 (2018) 128–138.
[110] Y. Li, L. Shi, X. Cai, H. Zhao, X. Niu, M. Lan, Electrochim. Acta 294 (2019) 304–311.
[111] T. Meng, L. Wang, H. Jia, T. Gong, Y. Feng, R. Li, H. Wang, Y. Zhang, J. Colloid Interf. Sci. 536 (2019) 424–430.
[112] X. Feng, X. Yin, X. Bo, L. Guo, Sens. Actuat. B 281 (2019) 730–738.
[113] J. Han, Y. Zhuo, Y.Q. Chai, Y. Xiang, R. Yuan, Anal. Chem. 87 (2015) 1669–1675.
[114] L. Wang, Q. Zhang, S. Chen, F. Xu, S. Chen, J. Jia, H. Tan, H. Hou, Y. Song, Anal. Chem. 86 (2014) 1414–1421.
[115] J. Han, M. Zhang, G. Chen, Y. Zhang, Q. Wei, Y. Zhuo, G. Xie, R. Yuan, S. Chen, J. Mater. Chem. B 5 (2017) 8330–8336.
[116] S. Li, Y. Duan, S. Lei, J. Qiao, G. Li, B. Ye, Sens. Actuators, B 274 (2018) 218–227.
[117] J. Chang, X. Wang, J. Wang, H. Li, F. Li, Anal. Chem. 91 (2019) 3604–3610.
[118] B. He, X. Dong, Sens. Actuat. B 294 (2019) 192–198.
[119] Z. Zeng, X. Fang, W. Miao, Y. Liu, T. Maiyalagan, S. Mao, ACS Sens. 4 (2019) 1934–1941.
[120] Y. Lin, Q. Zhou, J. Li, J. Shu, Z. Qiu, Y. Lin, D. Tang, Anal. Chem. 88 (2016) 1030–1038.
[121] T.Z. Liu, R. Hu, X. Zhang, K.L. Zhang, Y. Liu, X.B. Zhang, R.Y. Bai, D. Li, Y.H. Yang, Anal. Chem. 88 (2016) 12516–12523.
[122] J. Liu, Y. Shang, Q. Zhu, X. Zhang, J. Zheng, Microchim. Acta 186 (2019) 509.
[123] Y. Song, M. Xu, C. Gong, Y. Shen, L. Wang, Y. Xie, L. Wang, Sens. Actuators, B 257 (2018) 792–799.
[124] Y. Chen, X.Z. Meng, H.W. Gu, H.C. Yi, W.Y. Sun, Biosens. Bioelectron. 134 (2019) 117–122.
[125] X. Yang, J. Lv, Z. Yang, R. Yuan, Y. Chai, Anal. Chem. 89 (2017) 11636–11640.
[126] X. Liu, D. Huang, C. Lai, G. Zeng, L. Qin, H. Wang, H. Yi, B. Li, S. Liu, M. Zhang, R. Deng, Y. Fu, L. Li, W. Xue, S. Chen, Chem. Soc. Rev. 48 (2019) 5266–5302.
[127] D. Huang, X. Liu, C. Lai, L. Qin, C. Zhang, H. Yi, G. Zeng, B. Li, R. Deng, S. Liu, Y. Zhang, Microchim. Acta 186 (2018) 31.
[128] D. Zhao, T. Wang, D. Han, C. Rusinek, A.J. Steckl, W.R. Heineman, Anal. Chem. 87 (2015) 9315–9321.
[129] J. Wang, J. Lu, S.B. Hocevar, P.A.M. Farias, B. Ogorevc, Anal. Chem. 72 (2000) 3218–3222.
[130] C. Gao, X.J. Huang, TrAC, Trends Anal. Chem. 51 (2013) 1–12.
[131] Y. Wang, Y. Wu, J. Xie, X. Hu, Sens. Actuat. B 177 (2013) 1161–1166.
[132] D. Wang, Y. Ke, D. Guo, H. Guo, J. Chen, W. Weng, Sens. Actuat. B 216 (2015) 504–510.
[133] H. Guo, Z. Zheng, Y. Zhang, H. Lin, Q. Xu, Sens. Actuat. B 248 (2017) 430–436.
[134] J.C. Jin, J. Wu, G.P. Yang, Y.L. Wu, Y.Y. Wang, Chem. Commun. 52 (2016) 8475–8478.
[135] E. Shi, G. Yu, H. Lin, C. Liang, T. Zhang, F. Zhang, F. Qu, Microchim. Acta 186 (2019) 451.
[136] L. Xiao, H. Xu, S. Zhou, T. Song, H. Wang, S. Li, W. Gan, Q. Yuan, Electrochim. Acta 143 (2014) 143–151.
[137] M. Roushani, A. Valipour, Z. Saedi, Sens. Actuat. B 233 (2016) 419–425.
[138] Y. Wang, L. Wang, W. Huang, T. Zhang, X. Hu, J.A. Perman, S. Ma, J. Mater. Chem. A 5 (2017) 8385–8393.